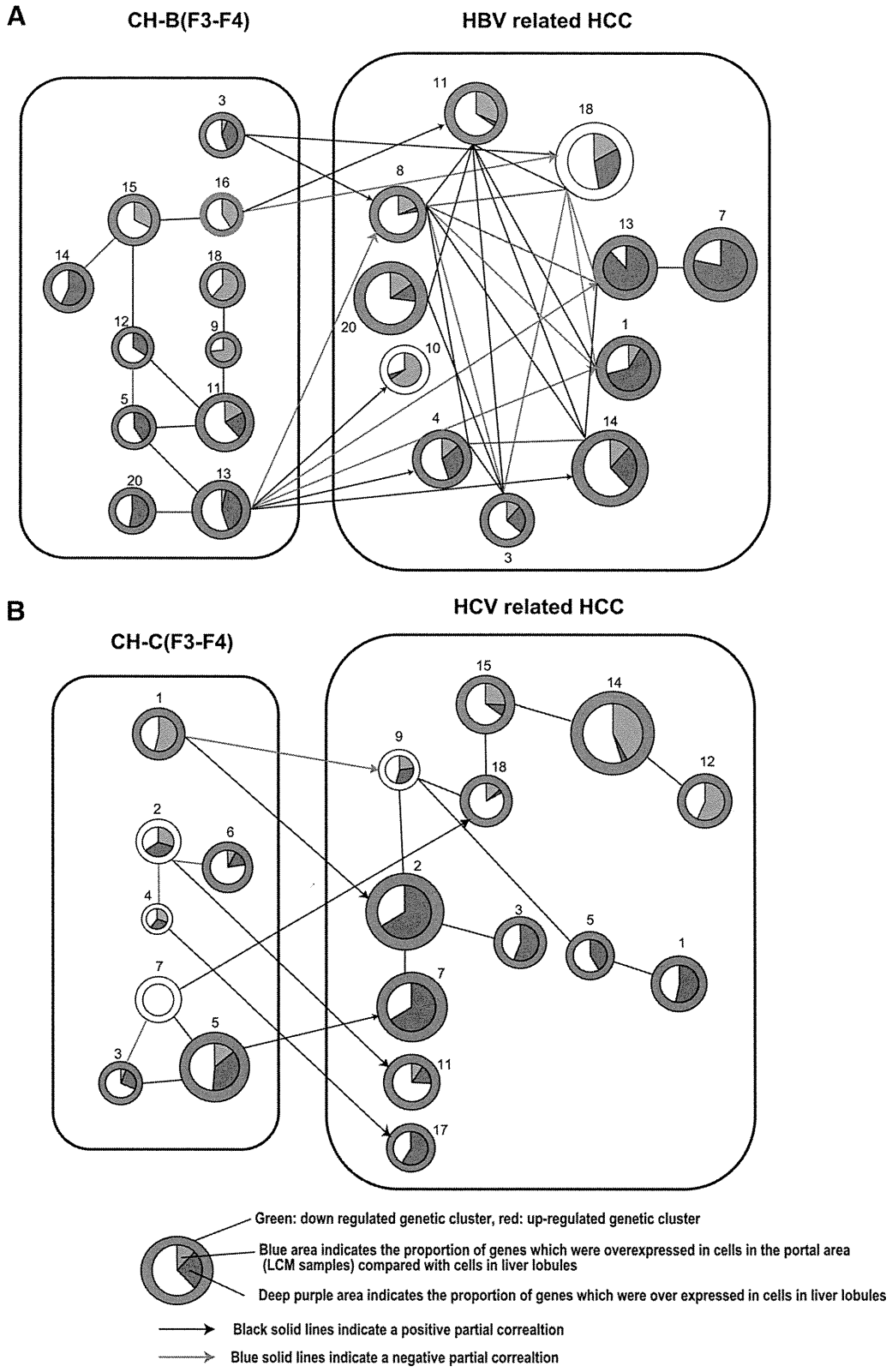

Fig. 3. GGM analysis of each cluster in HCC and non-cancerous lesions. Each cluster in the HCC and non-cancerous lesions was connected according to partial correlation coefficient matrix (PCCM) by GGM algorithms (Supplemental Tables H and I). The blue lines indicate a negative partial correlation and the black lines indicate a positive partial correlation. The size of each cluster reflects the number of clustered genes. The red circles are up-regulated gene clusters, while the green circles are down-regulated gene clusters. Within each cluster, the blue area indicates the proportion of genes that are over-expressed in CPA, while the deep purple area indicates the proportion of genes that are over-expressed in CLL. A; interactions of HBV related clusters. B; interactions of HCV related clusters.

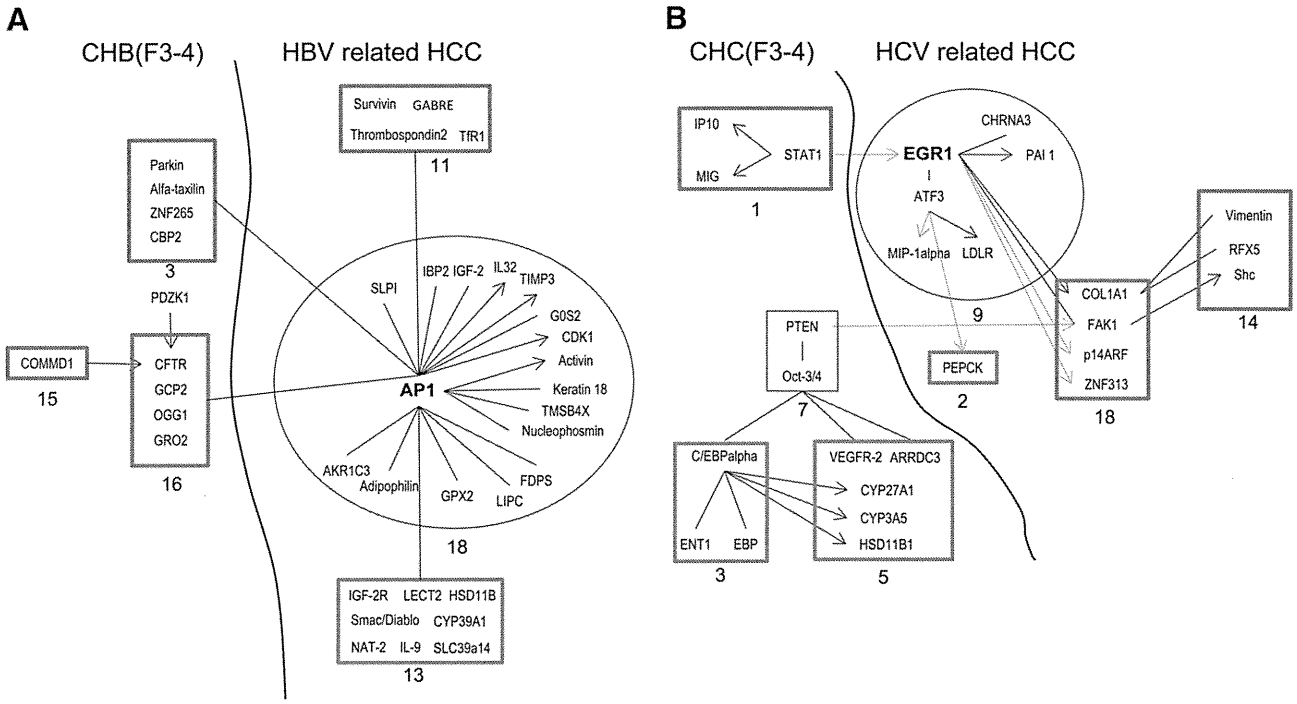

Fig. 4. Individual gene interactions between gene clusters in HCC and non-cancerous lesions. Direct interactions of individual genes among each cluster were confirmed by reference to the MetaCore database. The blue arrows indicate negative regulation, while the black arrows indicate positive regulation. Unspecified interactions are shown with black lines. The red squares are up-regulated gene clusters, while the green squares are down-regulated gene clusters. A; direct interactions of genes in HBV related clusters. B; direct interactions of genes in HCV related clusters.

GGM analysis between the HCC and non-cancerous liver revealed the unique interactions of 2 lesions in this study. In CH-B, up-regulated cluster Nos. 3 and 16, development and DNA damage response gene clusters, regulated HCC cluster Nos. 8, 11, and 18, VEGF-family signaling, apoptosis and survival-related, and ESR1 regulation of G1/S transition-related gene clusters. Down-regulated cluster No. 13, a metabolism-related gene cluster, negatively regulated the up-regulated HCC cluster No. 8. These results suggest that the metabolic status of non-cancerous liver influences the gene expression of HCC. Individual gene interactions with reference to the MetaCore database showed that 8 genes in non-cancerous cluster Nos. 3 and 16 were directly associated with AP1 in HCC cluster No. 18, which regulated the expression of many HCC genes (Fig. 4) [18–23]. Interestingly, the HBV transcript was clustered in HCC cluster No. 18. It has been reported that the HBV transcript enhances AP-1 activation [39,40]. The results suggest a role for the HBV transcript in CH-B-related HCC. Recently, a next generation sequencing approach revealed the frequent integration of HBV in HCC (86.4%), where the putative cancer-related human telomerase reverse transcriptase (hTERT), mixed-lineage leukemia 4, and cyclin E1 genes were located [41]. Although, we could not find the up-regulation of these genes in CH-B-related HCC, HBV genome integration should have important roles for HBV-related hepatocarcinogenesis. A previous report demonstrated that HBx retained the ability to overcome active oncogene RAS-induced senescence by using hTERT, which was introduced into human immortalized primary cells [42].

In CH-C, STAT1 and PTEN signaling in cluster Nos. 1 and 7, respectively, were associated with HCC cluster Nos. 9, 18, and 2, EGR1 signaling, ectodermal development and cell proliferation, lipid metabolism, and iron transport gene clusters. Individual gene interactions with reference to the MetaCore database showed that EGR1 regulates multiple genes in HCC cluster No. 9 as well as genes in up-regulated HCC cluster No. 18 and down-regulated HCC cluster No. 2 (Fig. 4). STAT1 and PTEN in non-cancerous cluster Nos. 1 and 7 exhibited an anti-tumor effect.

STAT1 negatively regulated EGR1 [24] and, interestingly, the expression of PTEN was associated with metabolic-related genes in non-cancerous cluster Nos. 3 and 5 (Fig. 4). PTEN reportedly promotes oxidative phosphorylation, decreases glycolysis, and prevents the metabolic reprogramming of cancer cells [43].

The reduced expression of these antitumor genes in CH-C might increase the expression of EGR1 and FAK1, which promote angiogenesis, fibrogenesis, and tumorigenesis in HCC (Fig. 4). EGR-1 promotes hepatocellular mitotic progression [44], while p53 and PTEN are downstream targets of EGR1. EGR1 might be involved in a negative feedback mechanism of cell cycle progression by inducing p53 and PTEN [45]. Recent reports described the tumorigenic role of EGR1 in the presence of p53 and PTEN mutations [46,47]. Thus, interferon signaling evoked by an innate immune response and the PTEN expression-associated metabolic process (Nos. 3 and 5) will likely regulate the gene expression profile of HCC through EGR1.

It is reported that HBV X protein represses the expression of PTEN by inhibiting the function of p53 [48] and c-Jun promotes cellular survival by suppression of PTEN [49]. In this study, the expression of PTEN was repressed in CH-B (Supplemental Fig. B, CH-B, cluster 21). Possible involvement of HBx, AP-1 and PTEN signaling in HBV-related hepatocarcinogenesis should be explored furthermore.

Recently, Hoshida et al. reported that gene expression profiling of the background liver of patients with HCC predicts their outcome [35]. In their report, gene sets, which correlated with good survival, included many metabolic process genes, such as those of fatty acid, amino acid, and glucose metabolism. In accordance with their results, our findings showed that the possible involvement of metabolic process genes in the background liver might influence gene expression in HCC. In addition, our study revealed the predisposing changes of gene expression in non-cancerous liver that precede the changes of gene expression in HCC. Interestingly, we found that the expression of the anti-tumor genes STAT1 and PTEN was decreased significantly at the onset of HCC compared with the tumor-free time. Therefore, serial analysis of the expression of these genes might be useful for predicting the development of HCC. Several reports have shown that the decreased expression of some chemokines, such as CXCL10, CCL2, and CCL5, is associated with the poor prognosis of resectable HCC [50,51]. In this study, the expression of CXCL10, CXCL6, CXCL9,

and macrophage migration inhibitory factor was decreased at the onset of HCC compared with the tumor-free time (Supplemental Fig. C). It would be worthwhile to examine the expression of these genes in serum samples to predict the development of HCC.

In summary, using a bioinformatics approach, we performed gene expression profiling of HCC and non-cancerous liver, which revealed the predisposing changes of gene expression in HCC. This approach will be useful for the early diagnosis of HCC. Further studies with a larger sample population are needed to confirm our data and to determine possible means for preventing the development of HCC.

4. Materials and methods

4.1. Patients and tissue samples

HCC and non-cancerous liver specimens were obtained from 17 patients with HCV-related HCC and 17 with HBV-related HCC who underwent surgical resection of the liver (Supplemental Tables A and B). For the control normal liver, a surgically obtained tissue sample from a patient who showed no clinical signs of hepatitis was used as described previously [9,10]. The liver tissue was histologically normal, and the patient tested negative for all hepatitis virus markers and had normal levels of serum aminotransferase. HCC and non-cancerous liver tissues were enucleated from resected specimens and frozen immediately in liquid nitrogen for RNA isolation [10]. In a previous study, expression profiling of the liver of 19 patients with CH-B and 18 with CH-C was performed (Table 2) [10]. The other experimental procedures are described in the Supplemental Materials and Methods.

4.2. Microarray analysis

cDNA microarray slides (Liver chip 10 k) were used as described previously [10]. For the selection of genes, we utilized data from the cDNA microarray and hepatic SAGE libraries derived from normal liver, CH-C, CH-C-related HCC, CH-B, and CH-B-related HCC, including 52,149 unique tags. We selected 9614 non-redundant genes that are expressed in diseased and normal liver. The detailed procedures for the preparation of the cDNA microarray slides are described in the Supplemental Material and Methods. RNA isolation, amplification of antisense RNA, labeling, and hybridization were performed according to the protocols described previously [10]. Quantitative assessment of the signals on the slides was performed by scanning on a ScanArray 5000 (General Scanning, Watertown, MA) followed by image analysis using GenePix Pro 4.1 (Axon Instruments, Union City, CA) as described previously [10]. The microarray data have been submitted to the Gene Expression Omnibus (GEO) public database at NCBI (Accession No. GSE41804). The details are also described in the Supplemental Material and Methods.

4.3. Graphical Gaussian modeling data processing

GGM [15,16] enabled us to reveal the gene cluster framework in relation to hepatocellular carcinogenesis of CH-B and CH-C. The procedure included: 1) gene clustering; 2) construction of the PCCM by GGM algorithms; and 3) visualization of the cluster pathway (Supplemental Fig. A).

4.4. Gene selection

To utilize a variety of tissue samples, we first calculated the ratio of gene expression in non-cancerous tissue (36 with CH-B and 35 with CH-C) to that in normal tissue and the ratio of gene expression in HCC tissue (17 with CH-B related HCC and 17 with CH-C related HCC) to that in normal tissue. Then, the expression ratios of non-cancerous and HCC tissues in individual samples were standardized in the two tissues, respectively, by transformation to the Z score (each value was subtracted by the average value and divided by the standard deviation (SD)) such that the mean expression value was 0 and the SD was 1. A gene was regarded as differentially expressed if the Z score was >1 or <-1 ($1 > |AV \pm SD|$). Although the criterion for a differentially expressed gene is usually $|AV \pm 2SD|$, the selection procedure described above is simply designed to gather as many differentially expressed genes as possible, and is suitable for determining the macroscopic relationships between gene systems estimated by cluster analysis. Gene selection from non-HCC samples was performed similarly by avoiding the selected genes in HCC (backward selection). Therefore, a correlation between HCC and non-HCC genes could be obtained as there was no overlap between the genes.

4.5. Clustering with automatic determination of cluster number

In gene profile clustering, the Euclidian distance between Pearson's correlation coefficient of profiles and the unweighted pair group method using the arithmetic average (UPGMA or group average method) were adopted as the metric and the technique, respectively, with reference to previous GGM analysis [15,16]. Note that the present metric and technique were selected to estimate robustly the clusters against the noise of gene expression measurements [15]. In cluster number estimation, the variance inflation factor was adopted as a stopping rule for the hierarchical clustering of expression profiles [15], and the popular cutoff value of 10.0 [52] was adopted as the threshold.

4.6. Graphical Gaussian modeling

The average expression profiles were calculated for the members of each cluster, and the average correlation coefficient matrix between the clusters was calculated. The average correlation coefficient matrix between the clusters was then subjected to GGM as described previously [15,16]. The correlation coefficient can return a false value in the presence of confounding factors. Partial correlation enables replacement of a false-positive correlation with the actual correlation. The PCCM was calculated using GGM (Supplemental Fig. A). All calculations for clustering analysis and GGM were performed via the ASIAN web site (http://eureka.cbrc.jp/asian/index_j.html) [53] and "Auto Net Finder," a commercial desktop version of ASIAN (Infocom Corporation, Shibuya, Tokyo, Japan, http://www.infocom.co.jp/bio/download/).

4.7. Rearrangement of the inferred network

Since the magnitude of the partial correlation coefficient indicates the strength of the association between clusters, the intact network can be rearranged according to the partial correlation coefficient to interpret the association between clusters. The strength of the association can be assigned by a standard test for the partial correlation coefficient. In the present study, the significance level in the *t*-test was 1% (Supplemental Fig. A).

4.8. Gene ontology of cluster members

Functional ontology enrichment analysis was performed to examine the gene ontology process distribution of each cluster gene using MetaCore™ (Thomson Reuters, New York, NY). Gene ontology was also confirmed by DAVID Bioinformatics Resources 6.7 (http://david.abcc.ncifcrf.gov/) [17].

Supplementary data to this article can be found online at http://dx.doi.org/10.1016/j.ygeno.2013.02.007.

Acknowledgments

The authors thank Nami Nishiyama for excellent technical assistance.

References

[1] R. Siegel, D. Naishadham, A. Jemal, Cancer statistics, 2012, CA Cancer J. Clin. 62 (2012) 10–29.

[2] H. Tsukuma, T. Hiyama, S. Tanaka, M. Nakao, T. Yabuuchi, T. Kitamura, K. Nakanishi, I. Fujimoto, A. Inoue, H. Yamazaki, Risk factors for hepatocellular carcinoma among patients with chronic liver disease, N. Engl. J. Med. 328 (1993) 1797–1801.

[3] A. Arzumanyan, H.M. Reis, M.A. Feitelson, Pathogenic mechanisms in HBV- and HCV-associated hepatocellular carcinoma, Nat. Rev. Cancer 13 (2012) 123–135.

[4] H. Yoshida, Y. Shiratori, M. Moriyama, Y. Arakawa, T. Ide, M. Sata, O. Inoue, M. Yano, M. Tanaka, S. Fujiyama, S. Nishiguchi, T. Kuroki, F. Imazeki, O. Yokosuka, S. Kinoyama, G. Yamada, M. Omata, Interferon therapy reduces the risk for hepatocellular carcinoma: national surveillance program of cirrhotic and noncirrhotic patients with chronic hepatitis C in Japan. IHIT Study Group. Inhibition of hepatocarcinogenesis by interferon therapy, Ann. Intern. Med. 131 (1999) 174–181.

[5] G. Fattovich, T. Stroffolini, I. Zagni, F. Donato, Hepatocellular carcinoma in cirrhosis: incidence and risk factors, Gastroenterology 127 (2004) S35–S50.

[6] A. de La Coste, B. Romagnolo, P. Billuart, C.A. Renard, M.A. Buendia, O. Soubrane, M. Fabre, J. Chelly, C. Beldjord, A. Kahn, C. Perret, Somatic mutations of the beta-catenin gene are frequent in mouse and human hepatocellular carcinomas, Proc. Natl. Acad. Sci. U. S. A. 95 (1998) 8847–8851.

[7] D.F. Calvisi, S. Ladu, A. Gorden, M. Farina, E.A. Conner, J.S. Lee, V.M. Factor, S.S. Thorgeirsson, Ubiquitous activation of Ras and Jak/Stat pathways in human HCC, Gastroenterology 130 (2006) 1117–1128.

[8] G.H. Thoresen, T.K. Guren, D. Sandnes, M. Peak, L. Agius, T. Christoffersen, Response to transforming growth factor alpha (TGFalpha) and epidermal growth factor (EGF) in hepatocytes: lower EGF receptor affinity of TGFalpha is associated with more sustained activation of p42/p44 mitogen-activated protein kinase and greater efficacy in stimulation of DNA synthesis, J. Cell. Physiol. 175 (1998) 10–18.

[9] M. Honda, S. Kaneko, H. Kawai, Y. Shirota, K. Kobayashi, Differential gene expression between chronic hepatitis B and C hepatic lesion, Gastroenterology 120 (2001) 955–966.

[10] M. Honda, T. Yamashita, T. Ueda, H. Takatori, R. Nishino, S. Kaneko, Different signaling pathways in the livers of patients with chronic hepatitis B or chronic hepatitis C, Hepatology 44 (2006) 1122–1138.

[11] M. Honda, M. Nakamura, M. Tateno, A. Sakai, T. Shimakami, T. Shirasaki, T. Yamashita, K. Arai, T. Yamashita, Y. Sakai, S. Kaneko, Differential interferon signaling in liver lobule and portal area cells under treatment for chronic hepatitis C, J. Hepatol. 53 (2010) 817–826.

[12] H. Kishino, P.J. Waddell, Correspondence analysis of genes and tissue types and finding genetic links from microarray data, Genome Inform. Ser. Workshop Genome Inform. 11 (2000) 83–95.

[13] P.J. Waddell, H. Kishino, Cluster inference methods and graphical models evaluated on NCI60 microarray gene expression data, Genome Inform. Ser. Workshop Genome Inform. 11 (2000) 129–140.

[14] J. Krumsiek, K. Suhre, T. Illig, J. Adamski, F.J. Theis, Gaussian graphical modeling reconstructs pathway reactions from high-throughput metabolomics data, BMC Syst. Biol. 5 (2011) 21.

[15] H. Toh, K. Horimoto, Inference of a genetic network by a combined approach of cluster analysis and graphical Gaussian modeling, Bioinformatics 18 (2002) 287–297.

[16] S. Aburatani, F. Sun, S. Saito, M. Honda, S. Kaneko, K. Horimoto, Gene systems network inferred from expression profiles in hepatocellular carcinogenesis by graphical Gaussian model, EURASIP J. Bioinform. Syst. Biol. (2007) 47214.

[17] W. Huang da, B.T. Sherman, Q. Tan, J. Kir, D. Liu, D. Bryant, Y. Guo, R. Stephens, M.W. Baseler, H.C. Lane, R.A. Lempicki, DAVID bioinformatics resources: expanded annotation database and novel algorithms to better extract biology from large gene lists, Nucleic Acids Res. 35 (2007) W169–W175.

[18] L. Russell, D.R. Forsdyke, A human putative lymphocyte G0/G1 switch gene containing a CpG-rich island encodes a small basic protein with the potential to be phosphorylated, DNA Cell Biol. 10 (1991) 581–591.

[19] L. Zhong, J. Ou, U. Barkai, J.F. Mao, J. Frasor, G. Gibori, Molecular cloning and characterization of the rat ovarian 20 alpha-hydroxysteroid dehydrogenase gene, Biochem. Biophys. Res. Commun. 249 (1998) 797–803.

[20] K.M. Mani, C. Lefebvre, K. Wang, W.K. Lim, K. Basso, R. Dalla-Favera, A. Califano, A systems biology approach to prediction of oncogenes and molecular perturbation targets in B-cell lymphomas, Mol. Syst. Biol. 4 (2008) 169.

[21] H.K. Kwon, J.S. Hwang, J.S. So, C.G. Lee, A. Sahoo, J.H. Ryu, W.K. Jeon, B.S. Ko, C.R. Im, S.H. Lee, Z.Y. Park, S.H. Im, Cinnamon extract induces tumor cell death through inhibition of NFkappaB and AP1, BMC Cancer 10 (2010) 392.

[22] K.R. Mitchell, D. Warshawsky, Xenobiotic inducible regions of the human arylamine N-acetyltransferase 1 and 2 genes, Toxicol. Lett. 139 (2003) 11–23.

[23] D. Bottomly, S.L. Kyler, S.K. McWeeney, G.S. Yochum, Identification of {beta}-catenin binding regions in colon cancer cells using ChIP-Seq, Nucleic Acids Res. 38 (2010) 5735–5745.

[24] J.L. Ingram, A. Antao-Menezes, J.B. Mangum, O. Lyght, P.J. Lee, J.A. Elias, J.C. Bonner, Opposing actions of Stat1 and Stat6 on IL-13-induced up-regulation of early growth response-1 and platelet-derived growth factor ligands in pulmonary fibroblasts, J. Immunol. 177 (2006) 4141–4148.

[25] H. Liao, M.C. Hyman, D.A. Lawrence, D.J. Pinsky, Molecular regulation of the PAI-1 gene by hypoxia: contributions of Egr-1, HIF-1alpha, and C/EBPalpha, FASEB J. 21 (2007) 935–949.

[26] V. Lejard, F. Blais, M.J. Guerquin, A. Bonnet, M.A. Bonnin, E. Havis, M. Malbouyres, C.B. Bidaud, G. Maro, P. Gilardi-Hebenstreit, J. Rossert, F. Ruggiero, D. Duprez, EGR1 and EGR2 involvement in vertebrate tendon differentiation, J. Biol. Chem. 286 (2011) 5855–5867.

[27] V. Golubovskaya, A. Kaur, W. Cance, Cloning and characterization of the promoter region of human focal adhesion kinase gene: nuclear factor kappa B and p53 binding sites, Biochim. Biophys. Acta 1678 (2004) 111–125.

[28] S.P. Berasi, C. Huard, D. Li, H.H. Shih, Y. Sun, W. Zhong, J.E. Paulsen, E.L. Brown, R.E. Gimeno, R.V. Martinez, Inhibition of gluconeogenesis through transcriptional activation of EGR1 and DUSP4 by AMP-activated kinase, J. Biol. Chem. 281 (2006) 27167–27177.

[29] J. Gu, M. Tamura, R. Pankov, E.H. Danen, T. Takino, K. Matsumoto, K.M. Yamada, Shc and FAK differentially regulate cell motility and directionality modulated by PTEN, J. Cell Biol. 146 (1999) 389–403.

[30] J.F. Rual, K. Venkatesan, T. Hao, T. Hirozane-Kishikawa, A. Dricot, N. Li, G.F. Berriz, F.D. Gibbons, M. Dreze, N. Ayivi-Guedehoussou, N. Klitgord, C. Simon, M. Boxem, S. Milstein, J. Rosenberg, D.S. Goldberg, L.V. Zhang, S.L. Wong, G. Franklin, S. Li, J.S. Albala, J. Lim, C. Fraughton, E. Llamosas, S. Cevik, C. Bex, P. Lamesch, R.S. Sikorski, J. Vandenhaute, H.Y. Zoghbi, A. Smolyar, S. Bosak, R. Sequerra, L. Doucette-Stamm, M.E. Cusick, D.E. Hill, F.P. Roth, M. Vidal, Towards a proteome-scale map of the human protein–protein interaction network, Nature 437 (2005) 1173–1178.

[31] T.P. Hecker, J.R. Grammer, G.Y. Gillespie, J. Stewart, C.L. Gladson, Focal adhesion kinase enhances signaling through the Shc/extracellular signal-regulated kinase pathway in anaplastic astrocytoma tumor biopsy samples, Cancer Res. 62 (2002) 2699–2707.

[32] H. Okabe, S. Satoh, T. Kato, O. Kitahara, R. Yanagawa, Y. Yamaoka, T. Tsunoda, Y. Furukawa, Y. Nakamura, Genome-wide analysis of gene expression in human hepatocellular carcinomas using cDNA microarray: identification of genes involved in viral carcinogenesis and tumor progression, Cancer Res. 61 (2001) 2129–2137.

[33] Y. Hippo, K. Watanabe, A. Watanabe, Y. Midorikawa, S. Yamamoto, S. Ihara, S. Tokita, H. Iwanari, Y. Ito, K. Nakano, J. Nezu, H. Tsunoda, T. Yoshino, I. Ohizumi, M. Tsuchiya, S. Ohnishi, M. Makuuchi, T. Hamakubo, T. Kodama, H. Aburatani, Identification of soluble NH2-terminal fragment of glypican-3 as a serological marker for early-stage hepatocellular carcinoma, Cancer Res. 64 (2004) 2418–2423.

[34] Y. Shirota, S. Kaneko, M. Honda, H.F. Kawai, K. Kobayashi, Identification of differentially expressed genes in hepatocellular carcinoma with cDNA microarrays, Hepatology 33 (2001) 832–840.

[35] Y. Hoshida, A. Villanueva, M. Kobayashi, J. Peix, D.Y. Chiang, A. Camargo, S. Gupta, J. Moore, M.J. Wrobel, J. Lerner, M. Reich, J.A. Chan, J.N. Glickman, K. Ikeda, M. Hashimoto, G. Watanabe, M.G. Daidone, S. Roayaie, M. Schwartz, S. Thung, H.B. Salvesen, S. Gabriel, V. Mazzaferro, J. Bruix, S.L. Friedman, H. Kumada, J.M. Llovet, T.R. Golub, Gene expression in fixed tissues and outcome in hepatocellular carcinoma, N. Engl. J. Med. 359 (2008) 1995–2004.

[36] L. Xia, W. Huang, D. Tian, H. Zhu, Y. Zhang, H. Hu, D. Fan, Y. Nie, K. Wu, Upregulated FoxM1 expression induced by hepatitis B virus X protein promotes tumor metastasis and indicates poor prognosis in hepatitis B virus-related hepatocellular carcinoma, J. Hepatol. 57 (2012) 600–612.

[37] S. Ura, M. Honda, T. Yamashita, T. Ueda, H. Takatori, R. Nishino, H. Sunakozaka, Y. Sakai, K. Horimoto, S. Kaneko, Differential microRNA expression between hepatitis B and hepatitis C leading disease progression to hepatocellular carcinoma, Hepatology 49 (2009) 1098–1112.

[38] R. Turner, O. Lozoya, Y. Wang, V. Cardinale, E. Gaudio, G. Alpini, G. Mendel, E. Wauthier, C. Barbier, D. Alvaro, L.M. Reid, Human hepatic stem cell and maturational liver lineage biology, Hepatology 53 (2011) 1035–1045.

[39] K.M. Sze, G.K. Chu, J.M. Lee, I.O. Ng, C-terminal truncated HBx is associated with metastasis and enhances invasiveness via C-Jun / MMP10 activation in hepatocellular carcinoma, Hepatology (2012).

[40] Y. Tanaka, F. Kanai, T. Ichimura, K. Tateishi, Y. Asaoka, B. Guleng, A. Jazag, M. Ohta, J. Imamura, T. Ikenoue, H. Ijichi, T. Kawabe, T. Isobe, M. Omata, The hepatitis B virus X protein enhances AP-1 activation through interaction with Jab1, Oncogene 25 (2006) 633–642.

[41] W.K. Sung, H. Zheng, S. Li, R. Chen, X. Liu, Y. Li, N.P. Lee, W.H. Lee, P.N. Ariyaratne, C. Tennakoon, F.H. Mulawadi, K.F. Wong, A.M. Liu, R.T. Poon, S.T. Fan, K.L. Chan, Z. Gong, Y. Hu, Z. Lin, G. Wang, Q. Zhang, T.D. Barber, W.C. Chou, A. Aggarwal, K. Hao, W. Zhou, C. Zhang, J. Hardwick, C. Buser, J. Xu, Z. Kan, H. Dai, M. Mao, C. Reinhard, J. Wang, J.M. Luk, Genome-wide survey of recurrent HBV integration in hepatocellular carcinoma, Nat. Genet. 44 (2012) 765–769.

[42] N. Oishi, K. Shilagardi, Y. Nakamoto, M. Honda, S. Kaneko, S. Murakami, Hepatitis B virus X protein overcomes oncogenic RAS-induced senescence in human immortalized cells, Cancer Sci. 98 (2007) 1540–1548.

[43] A. Ortega-Molina, M. Serrano, PTEN in cancer, metabolism, and aging, Trends Endocrinol. Metab. (2012).

[44] Y. Liao, O.N. Shikapwashya, E. Shteyer, B.K. Dieckgraefe, P.W. Hruz, D.A. Rudnick, Delayed hepatocellular mitotic progression and impaired liver regeneration in early growth response-1-deficient mice, J. Biol. Chem. 279 (2004) 43107–43116.

[45] Y. Zwang, A. Sas-Chen, Y. Drier, T. Shay, R. Avraham, M. Lauriola, E. Shema, E. Lidor-Nili, J. Jacob-Hirsch, N. Amariglio, Y. Lu, G.B. Mills, G. Rechavi, M. Oren, E. Domany, Y. Yarden, Two phases of mitogenic signaling unveil roles for p53 and EGR1 in elimination of inconsistent growth signals, Mol. Cell 42 (2011) 524–535.

[46] J. Yu, S.S. Zhang, K. Saito, S. Williams, Y. Arimura, Y. Ma, Y. Ke, V. Baron, D. Mercola, G.S. Feng, E. Adamson, T. Mustelin, PTEN regulation by Akt-EGR1-ARF-PTEN axis, EMBO J. 28 (2009) 21–33.

[47] D. Lu, C. Han, T. Wu, Microsomal prostaglandin E synthase-1 promotes hepatocarcinogenesis through activation of a novel EGR1/beta-catenin signaling axis, Oncogene 31 (2012) 842–857.

[48] T.W. Chung, Y.C. Lee, J.H. Ko, C.H. Kim, Hepatitis B Virus X protein modulates the expression of PTEN by inhibiting the function of p53, a transcriptional activator in liver cells, Cancer Res. 63 (2003) 3453–3458.

[49] K. Hettinger, F. Vikhanskaya, M.K. Poh, M.K. Lee, I. de Belle, J.T. Zhang, S.A. Reddy, K. Sabapathy, c-Jun promotes cellular survival by suppression of PTEN, Cell Death Differ. 14 (2007) 218–229.

[50] V. Chew, C. Tow, M. Teo, H.L. Wong, J. Chan, A. Gehring, M. Loh, A. Bolze, R. Quek, V.K. Lee, K.H. Lee, J.P. Abastado, H.C. Toh, A. Nardin, Inflammatory tumour microenvironment is associated with superior survival in hepatocellular carcinoma patients, J. Hepatol. 52 (2010) 370–379.
[51] V. Chew, J. Chen, D. Lee, E. Loh, J. Lee, K.H. Lim, A. Weber, K. Slankamenac, R.T. Poon, H. Yang, L.L. Ooi, H.C. Toh, M. Heikenwalder, I.O. Ng, A. Nardin, J.P. Abastado, Chemokine-driven lymphocyte infiltration: an early intratumoural event determining long-term survival in resectable hepatocellular carcinoma, Gut 61 (2012) 427–438.
[52] R.J. Freund, W.J. Wilson, Regression analysis : statistical modeling of a response variable, Academic Press, San Diego, 1998.
[53] S. Aburatani, K. Goto, S. Saito, H. Toh, K. Horimoto, ASIAN: a web server for inferring a regulatory network framework from gene expression profiles, Nucleic Acids Res. 33 (2005) W659–W664.

HEPATOLOGY
Official Journal of the American Association for the Study of Liver Diseases

Discrete Nature of EpCAM$^+$ and CD90$^+$ Cancer Stem Cells in Human Hepatocellular Carcinoma

Taro Yamashita,[1] Masao Honda,[1] Yasunari Nakamoto,[1] Masayo Baba,[1] Kouki Nio,[1] Yasumasa Hara,[1] Sha Sha Zeng,[1] Takehiro Hayashi,[1] Mitsumasa Kondo,[1] Hajime Takatori,[1] Tatsuya Yamashita,[1] Eishiro Mizukoshi,[1] Hiroko Ikeda,[1] Yoh Zen,[1] Hiroyuki Takamura,[1] Xin Wei Wang,[2] and Shuichi Kaneko[1]

Recent evidence suggests that hepatocellular carcinoma (HCC) is organized by a subset of cells with stem cell features (cancer stem cells; CSCs). CSCs are considered a pivotal target for the eradication of cancer, and liver CSCs have been identified by the use of various stem cell markers. However, little information is known about the expression patterns and characteristics of marker-positive CSCs, hampering the development of personalized CSC-targeted therapy. Here, we show that CSC markers EpCAM and CD90 are independently expressed in liver cancer. In primary HCC, EpCAM$^+$ and CD90$^+$ cells resided distinctively, and gene-expression analysis of sorted cells suggested that EpCAM$^+$ cells had features of epithelial cells, whereas CD90$^+$ cells had those of vascular endothelial cells. Clinicopathological analysis indicated that the presence of EpCAM$^+$ cells was associated with poorly differentiated morphology and high serum alpha-fetoprotein (AFP), whereas the presence of CD90$^+$ cells was associated with a high incidence of distant organ metastasis. Serial xenotransplantation of EpCAM$^+$/CD90$^+$ cells from primary HCCs in immune-deficient mice revealed rapid growth of EpCAM$^+$ cells in the subcutaneous lesion and a highly metastatic capacity of CD90$^+$ cells in the lung. In cell lines, CD90$^+$ cells showed abundant expression of c-Kit and *in vitro* chemosensitivity to imatinib mesylate. Furthermore, CD90$^+$ cells enhanced the motility of EpCAM$^+$ cells when cocultured *in vitro* through the activation of transforming growth factor beta (TGF-β) signaling, whereas imatinib mesylate suppressed *TGFB1* expression in CD90$^+$ cells as well as CD90$^+$ cell-induced motility of EpCAM$^+$ cells. *Conclusion*: Our data suggest the discrete nature and potential interaction of EpCAM$^+$ and CD90$^+$ CSCs with specific gene-expression patterns and chemosensitivity to molecular targeted therapy. The presence of distinct CSCs may determine the clinical outcome of HCC. (HEPATOLOGY 2013;57:1484-1497)

The cancer stem cell (CSC) hypothesis, which suggests that a subset of cells bearing stem-cell–like features is indispensable for tumor development, has recently been put forward subsequent to advances in molecular and stem cell biology. Liver cancer, including hepatocellular carcinoma (HCC), is a leading cause of cancer death worldwide.[1] Recent studies have shown the existence of CSCs in liver cancer cell lines and primary HCC specimens using various stem cell markers.[2-7] Independently, we have identified novel HCC subtypes defined by the hepatic stem/progenitor cell markers,

Abbreviations: 5-FU, fluorouracil; Abs, antibodies; AFP, alpha-fetoprotein; CK-19, cytokeratin-19; CSC, cancer stem cell; DNs, dysplastic nodules; EMT, epithelial mesenchymal transition; EpCAM; epithelial cell adhesion molecule; FACS, fluorescent-activated cell sorting; HBV, hepatitis B virus; HCC, hepatocellular carcinoma; HCV, hepatitis C virus; HSCs, hepatic stem cells; IF, immunofluorescence; IHC, immunohistochemistry; IR, immunoreactivity; MDS, multidimensional scaling; NBNC, non-B, non-C hepatitis; NOD/SCID, nonobese diabetic, severe combined immunodeficient; NT, nontumor; OV-1, ovalbumin 1; qPCR, quantitative real-time polymerase chain reaction; SC, subcutaneous; Smad3, Mothers against decapentaplegic homolog 3; TECs, tumor epithelial cells; TGF-β, transforming growth factor beta; T/N, tumor/nontumor; VECs, vascular endothelial cells; VM, vasculogenic mimicry; VEGFR, vascular endothelial growth factor receptor.

From the [1]Liver Center, Kanazawa University Hospital, Kanazawa, Ishikawa, Japan; and [2]Laboratory of Human Carcinogenesis, Center for Cancer Research, National Cancer Institute, Bethesda, MD.

Received July 9, 2012; revised October 22, 2012; accepted November 6, 2012.

This study was supported by a Grant-in-Aid from the Ministry of Education, Culture, Sports, Science, and Technology of Japan (23590967), a grant from the Japanese Society of Gastroenterology, a grant from the Ministry of Health, Labor, and Welfare, and a grant from the National Cancer Center Research and Development Fund (23-B-5) of Japan. X.W.W. is supported by the Intramural Research Program of the Center for Cancer Research, U.S. National Cancer Institute.

epithelial cell adhesion molecule (EpCAM) and alpha-fetoprotein (AFP), which correlate with distinct gene-expression signatures and prognosis.[8,9] EpCAM$^+$ HCC cells isolated from primary HCC and cell lines show CSC features, including tumorigenicity, invasiveness, and resistance to fluorouracil (5-FU).[10] Similarly, other groups have shown that CD133$^+$, CD90$^+$, and CD13$^+$ HCC cells are also CSCs, and that EpCAM, CD90, and CD133 are the only markers confirmed to enrich CSCs from primary HCCs thus far.[3-5,10]

Although EpCAM$^+$, CD90$^+$, and CD133$^+$ cells show CSC features, such as high tumorigenicity, an invasive nature, and resistance to chemo- and radiation therapy, it remains unclear whether these cells represent an identical HCC population and whether they share similar or distinct characteristics. In this study, we used fluorescent-activated cell sorting (FACS), microarray, and immunohistochemistry (IHC) techniques to investigate the expression patterns of the representative liver CSC markers CD133, CD90, and EpCAM in a total of 340 HCC cases and 7 cases of mesenchymal liver tumors. We further explored gene- and protein-expression patterns as well as tumorigenic capacity of sorted cells isolated from 15 primary HCCs and 7 liver cancer cell lines in an attempt to identify the molecular portraits of each cell type.

Materials and Methods

Clinical Specimens. HCC samples were obtained with informed consent from patients who had undergone radical resection at the Liver Center in Kanazawa University Hospital (Kanazawa, Japan), and tissue acquisition procedures were approved by the ethics committee of Kanazawa University. A total of 102 formalin-fixed and paraffin-embedded HCC samples, obtained from 2001 to 2007, were used for IHC analyses. Fifteen fresh HCC samples were obtained between 2008 and 2012 from surgically resected specimens and an autopsy specimen and were used immediately to prepare single-cell suspensions and xenotransplantation (Table 1). Seven hepatic stromal tumors (three cavernous hemangioma, two hemangioendothelioma, and two angiomyolipoma) were formalin fixed and paraffin embedded and used for IHC analyses.

Table 1. Clinicopathological Characteristics of HCC Cases Used for Xenotransplantation

ID	Age/ Sex	Etiology	Tumor Size (cm)	Histological Grade	AFP (ng/mL)	DCP (IU/mL)
P1	77/M	Alcohol	12.0	Moderate	198	322
P2	61/F	NBNC	11.0	Moderate	12	3,291
P3	66/M	NBNC	2.2	Moderate	13	45
P4	65/M	HCV	4.2	Poor	13,700	25,977
P5	52/M	HBV	6.0	Moderate	29,830	1,177
P6	60/M	HCV	2.7	Poor	249	185
P7	79/F	HBV	4.0	Poor	46,410	384
P8	77/F	NBNC	5.5	Moderate	17,590	562
P9	71/M	Alcohol	7.0	Poor	3,814	607
P10	51/M	HBV	2.2	Well	<10	21
P11	71/M	Alcohol	2.1	Well	<10	11
P12	60/M	HBV	10.8	Poor	323	2,359
P13	66/M	HCV	2.8	Moderate	11	29
P14	71/M	HCV	7.2	Moderate	235,700	375,080
P15	75/M	HBV	5.5	Poor	<10	97

Abbreviation: DCP, des-gamma-carboxy prothrombin.

Additional details of experimental procedures are available in the Supporting Information.

Results

EpCAM, CD133, and CD90 Expression in HCC. We first evaluated the frequencies of three representative CSC markers (EpCAM$^+$, CD90$^+$, and CD133$^+$ cells) in 12 fresh primary HCC cases surgically resected by FACS (representative data shown in Fig. 1A). Clinicopathological characteristics of primary HCC cases are shown in Table 1. We noted that frequency of EpCAM$^+$, CD90$^+$, and CD133$^+$ cells varied between individuals. Abundant CD90$^+$ (7.0%), but almost no EpCAM$^+$, cells (0.06%, comparable to the isotype control) were detected in P2, whereas few CD90$^+$ (0.6%), but abundant EpCAM$^+$, cells (17.5%) were detected in P4. Very small populations of EpCAM$^+$ (0.09%), CD90$^+$ (0.04%), and CD133$^+$ cells (0.05%) were found in P12, but they were almost nonexistent in P8, except for CD90$^+$ cells (0.08%) (Fig. 1A). We further evaluated the expression of EpCAM, CD90, and CD133 in xenografts obtained from surgically resected samples (P13 and P15) and an autopsy sample (P14). As a whole, compared to the isotype control, 7 of 15 HCCs contained definite EpCAM$^+$ cells (46.7%), whereas only 3 HCCs

Address reprint requests to: Taro Yamashita, M.D., Ph.D., Department of General Medicine, Kanazawa University Hospital, 13-1 Takara-Machi, Kanazawa, Ishikawa 920-8641, Japan. E-mail: taroy@m-kanazawa.jp; fax: +81-76-234-4250.

View this article online at wileyonlinelibrary.com.
DOI 10.1002/hep.26168
Potential conflict of interest: Nothing to report.
Additional Supporting Information may be found in the online version of this article.

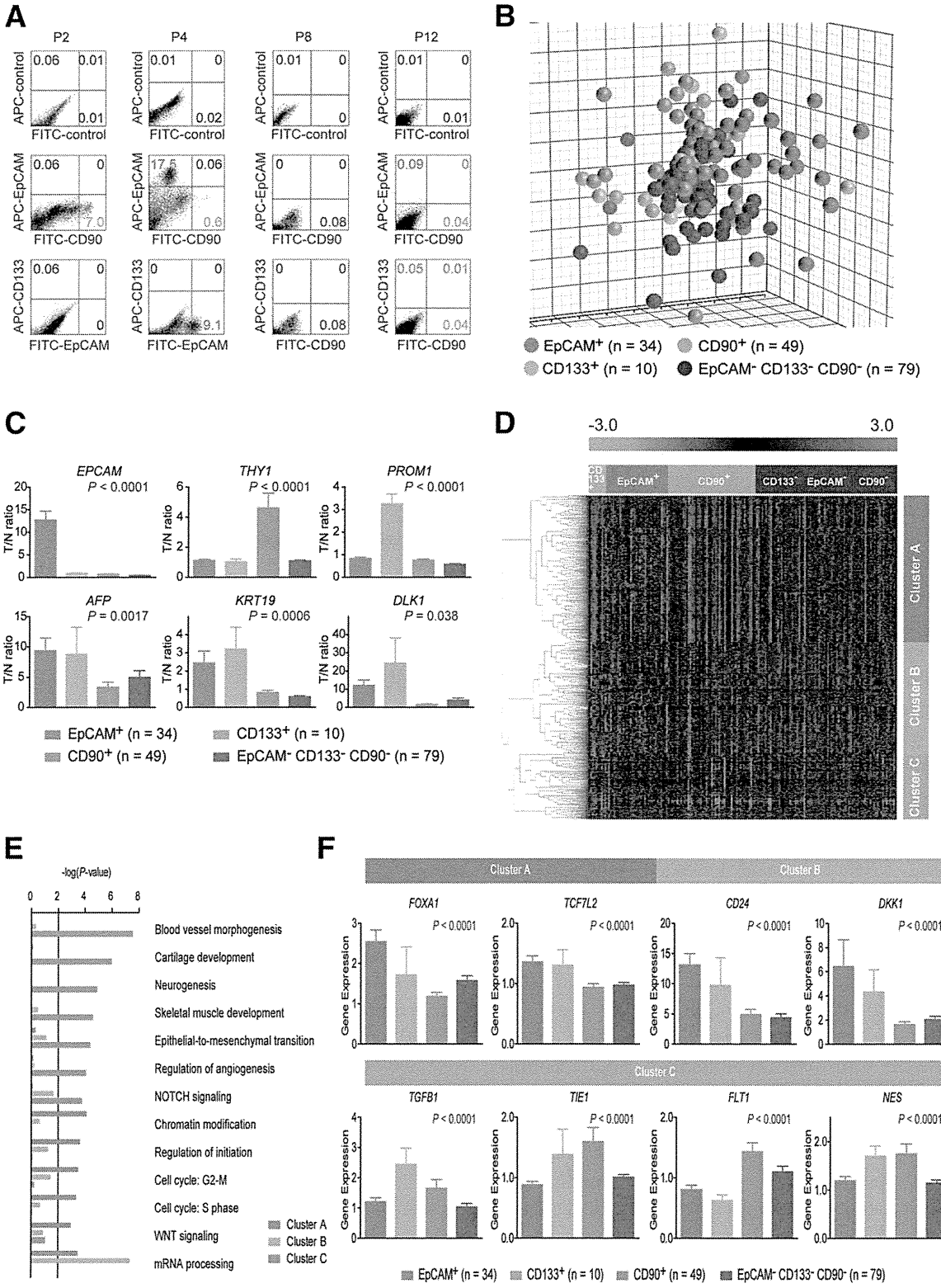

Fig. 1. Gene-expression profiles of CSC marker-positive HCCs. (A) FACS analysis of primary HCCs stained with fluorescent-labeled Abs against EpCAM, CD90, or CD133. (B) Multidimensional scaling analysis of 172 HCC cases characterized by the expression patterns of EpCAM, CD133, and CD90. Red, $EpCAM^+$ $CD90^-$ $CD133^-$ (n = 34); orange, $EpCAM^-$ $CD90^-$ $CD133^+$ (n = 10); light blue, $EpCAM^-$ $CD90^+$ $CD133^-$ (n = 49); blue, $EpCAM^-$ $CD90^-$ $CD133^-$ (n = 79). HCC specimens were clustered in specific groups with statistical significance ($P < 0.001$). (C) Expression patterns of well-known hepatic stem/progenitor markers in each HCC subtype, as analyzed by microarray. Red bar, $EpCAM^+$; orange bar, $CD133^+$; light blue bar, $CD90^+$; blue bar, $EpCAM^-$ $CD90^-$ $CD133^-$. (D) Hierarchical cluster analysis based on 1,561 EpCAM/CD90/CD133-coregulated genes in 172 HCC cases. Each cell in the matrix represents the expression level of a gene in an individual sample. Red and green cells depict high and low expression levels, respectively, as indicated by the scale bar. (E) Pathway analysis of EpCAM/CD90/CD133-coregulated genes. Canonical signaling pathways activated in cluster A (red bar), cluster B (orange bar), or cluster C (light blue bar) with statistical significance ($P < 0.01$) are shown. (F) Expression patterns of representative genes differentially expressed in EpCAM/CD90/CD133 HCC subtypes. Red bar, $EpCAM^+$; orange bar, $CD133^+$; light blue bar, $CD90^+$; blue bar, $EpCAM^-$ $CD133^-$ $CD90^-$.

Table 2. Tumorigenic Capacity of Unsorted, EpCAM$^+$, EpCAM$^-$, CD90$^+$, and CD90$^-$ Cells From Primary HCCs and Xenografts

Sample	CD133 (%)	CD90 (%)	EpCAM (%)	Cell Surface Marker	Number of Cells	Tumor Formation 2M	Tumor Formation 3M
P1	0	3.1	0	Unsorted	1×10^7	0/5	0/5
				CD90$^+$	1×10^5	0/5	0/5
				CD90$^-$	1×10^5	0/5	0/5
P2	0.06	7.0	0.06	Unsorted	1×10^7	0/5	0/5
				CD90$^+$	1×10^5	0/5	0/5
				CD90$^-$	1×10^5	0/5	0/5
P3	0	1.3	0	Unsorted	1×10^6	0/2	0/2
				CD90$^+$	1×10^4	0/4	0/4
				CD90$^-$	1×10^4	0/4	0/4
P4	0	0.6	17.5	Unsorted	1×10^6	3/4	4/4
				EpCAM$^+$	1×10^3	0/3	2/3
					1×10^4	3/4	4/4
					1×10^5	3/3	3/3
				CD90$^+$	1×10^3	0/3	0/3
					1×10^4	0/4	0/4
					1×10^5	0/3	0/3
				EpCAM$^-$ CD90$^-$	1×10^3	0/3	0/3
					1×10^4	0/4	0/4
					1×10^5	0/3	0/3
P5	0	0.8	29.7	Unsorted	1×10^6	0/5	0/5
				EpCAM$^+$	1×10^5	0/5	0/5
				CD90$^+$	1×10^5	0/5	0/5
				EpCAM$^-$ CD90$^-$	1×10^5	0/5	0/5
P6	0	0.7	0	Unsorted	1×10^6	0/2	0/2
				CD90$^+$	1×10^4	0/4	0/4
				CD90$^-$	1×10^4	0/4	0/4
P7	1.38	4.5	4.4	Unsorted	1×10^6	2/2	2/2
				EpCAM$^+$	2×10^2	0/3	0/3
					1×10^3	0/3	1/3
					1×10^4	2/4	4/4
				CD90$^+$	2×10^2	0/3	0/3
					1×10^3	0/3	0/3
					1×10^4	0/4	0/4
				EpCAM$^-$ CD90$^-$	1×10^3	0/3	0/3
					1×10^4	0/3	0/3
					1×10^5	0/4	0/4
P8	0	0.08	0	Unsorted	1×10^5	0/4	0/4
				CD90$^+$	1×10^3	0/3	0/3
				CD90$^-$	1×10^5	0/3	0/3
P9	0	0.26	0	Unsorted	1×10^5	0/4	0/4
				CD90$^+$	1×10^3	0/3	0/3
				CD90$^-$	1×10^5	0/3	0/3
P10	0	0.78	0	Unsorted	1×10^4	0/4	0/4
				CD90$^+$	1×10^3	0/3	0/3
				CD90$^-$	1×10^4	0/3	0/3
P11	0	0.1	1.54	Unsorted	5×10^4	0/2	0/2
				EpCAM$^+$	1×10^3	0/3	0/3
				CD90$^+$	1×10^3	0/3	0/3
				EpCAM$^-$ CD90$^-$	1×10^4	0/3	0/3
P12	0.06	0.05	0.09	Unsorted	1×10^5	0/3	3/3
				CD90$^+$	1×10^3	0/4	1/4
				CD90$^-$	1×10^3	0/4	1/4
					1×10^4	0/3	3/3
P13	0	0.03	67.7	EpCAM$^+$	5×10^5	4/4	NA
					5×10^4	3/3	NA
					5×10^3	3/3	NA
				EpCAM$^-$	5×10^5	0/4	NA
					5×10^4	0/3	NA
					5×10^3	0/3	NA
P14	24.0	0.06	3.1	EpCAM$^+$	5×10^3	4/5	NA
				EpCAM$^-$	5×10^3	2/5	NA
P15	0	2.45	0	CD90$^+$	5×10^4	3/4	NA
					5×10^3	1/3	NA
					5×10^2	1/3	NA
				CD90$^-$	5×10^4	2/4	NA
					5×10^3	1/3	NA
					5×10^2	0/3	NA

NA, not available.

contained definite CD133$^+$ cells (20%) (Table 2). CD90$^+$ cells were detected at variable frequencies in all 15 HCCs analyzed.

To explore the status of these CSC marker-positive cells in HCC in a large cohort, we utilized oligo-DNA microarray data from 238 HCC cases (GEO accession no.: GSE5975) to evaluate the expression of *EPCAM* (encoding EpCAM and CD326), *THY1* (encoding CD90), and *PROM1* (encoding CD133) in whole HCC tissues and nontumor (NT) tissues. Because previous studies demonstrated that CD133$^+$ and CD90$^+$ cells were detected at low frequency (~13.6% by CD133 staining and ~6.2% by CD90 staining) in HCC, but were almost nonexistent in NT liver (4, 5),[4,5] we utilized tumor/nontumor (T/N) gene-expression ratios to detect the existence of marker-positive CSCs in tumor. Accordingly, we showed that a 2-fold cutoff of T/N ratios of *EPCAM* successfully stratifies HCC samples with EpCAM$^+$ liver CSCs.[9,10]

A total of 95 (39.9%), 110 (46.2%), and 31 (13.0%) of the 238 HCC cases were thus regarded as EpCAM$^+$, CD90$^+$, and CD133$^+$ HCCs (T/N ratios: $\geq$2.0), respectively. As observed in the FACS data described above, we detected coexpression of EpCAM and CD90 in 45 HCCs (18.9%), EpCAM and CD133 in five HCCs (2%), CD90 and CD133 in five HCCs (2%), and EpCAM, CD90, and CD133 in 11 HCCs (4.6%). To clarify the characteristics of gene-expression signatures specific to stem cell marker expression status, we selected 172 HCC cases expressing a single CSC marker (34 EpCAM$^+$ CD90$^-$ CD133$^-$, 49 EpCAM$^-$ CD90$^+$ CD133$^-$, and 10 EpCAM$^-$ CD90$^-$ CD133$^+$) or all marker-negative HCCs (79 EpCAM$^-$ CD90$^-$ CD133$^-$). A class-comparison analysis with

univariate F tests and a global permutation test (×10,000) yielded a total of 1,561 differentially expressed genes. Multidimensional scaling (MDS) analysis using this gene set indicated that HCC specimens were clustered in specific groups with statistical significance ($P < 0.001$). Close examination of MDS plots revealed three major HCC subtype clusters: all marker-negative HCCs (blue spheres); EpCAM single-positive HCCs (red spheres); and CD90 single-positive HCCs (light blue spheres). $CD133^+$ HCCs (orange spheres) were rare, relatively scattered, and not clustered (Fig. 1B).

We examined the expression of representative hepatic stem/progenitor cell markers *AFP*, *KRT19*, and *DLK1* in HCCs with regard to the gene-expression status of each CSC marker (Fig. 1C). All three markers were up-regulated in $EpCAM^+$ and $CD133^+$ HCCs, compared with all marker-negative HCCs, consistent with previous findings.[10,11] However, we found no significant overexpression of *AFP*, *KRT19*, and *DLK1* in $CD90^+$ and all marker-negative HCCs.

Hierarchical cluster analyses revealed three main gene clusters that were up-regulated in $EpCAM^+$ HCCs (cluster A, 706 genes), $EpCAM^+$ or $CD133^+$ HCCs (cluster B, 530 genes), and $CD90^+$ or $CD133^+$ HCCs (cluster C, 325 genes) (Fig. 1D). Pathway analysis indicated that the enriched genes in cluster A (red bar) were associated with chromatin modification, cell-cycle regulation, and Wnt/β-catenin signaling (Fig. 1E). Genes associated with messenger RNA processing were enriched in clusters A (red bar) and B (orange bar). Surprisingly, genes in cluster C were significantly associated with pathways involved in blood-vessel morphogenesis, angiogenesis, neurogenesis, and epithelial mesenchymal transition (EMT) (light blue bar). Close examination of genes in each cluster suggested that known hepatic transcription factors (*FOXA1*), Wnt regulators (*TCF7L2* and *DKK1*), and a hepatic stem cell marker (*CD24*) were dominantly up-regulated in $EpCAM^+$ and $CD133^+$ HCCs (Fig. 1F). By contrast, genes associated with blood-vessel morphogenesis (*TIE1* and *FLT1*), EMT (*TGFB1*), and neurogenesis (*NES*) were activated dominantly in $CD90^+$ HCCs and $CD133^+$ HCCs.

$CD90^+$ HCC Cells Share Features With Mesenchymal Vascular Endothelial Cells. Because $CD133^+$ HCCs were relatively rare and constituted only 13% (microarray cohort) to 20% (FACS cohort) of all HCC samples analyzed, we focused on the characterization of EpCAM and CD90. To clarify the cell identity of $EpCAM^+$ or $CD90^+$ cells in primary HCCs, we performed IHC analysis of 18 needle-biopsy specimens of premalignant dysplastic nodules (DNs), 102 surgically resected HCCs, and corresponding NT liver tissues. When examining the expression of EpCAM and CD90 in cirrhotic liver tissue by double-color IHC analysis, we found that $EpCAM^+$ cells and $CD90^+$ cells were distinctively located and not colocalized (Supporting Fig. 1A). Immunoreactivity (IR) to anti-CD90 antibodies (Abs) was detected in vascular endothelial cells (VECs), inflammatory cells, fibroblasts, and neurons, but not in hepatocytes or cholangiocytes, in the cirrhotic liver (Supporting Fig. 1B, panels a,b). IR to anti-EpCAM Abs was detected in hepatic progenitors adjacent to the periportal area and bile duct epithelial cells in liver cirrhosis (Supporting Fig. 1B, panels c,d).

IR to anti-EpCAM Abs was detected in 37 of 102 surgically resected HCCs (Fig. 2A, panel b), but not in 18 DNs (Fig. 2A, panel a). By contrast, no tumor epithelial cells (TECs) showing IR to anti-CD90 Abs were found in any of the 18 DNs or 102 HCCs examined (Fig. 2A, panels c,d). However, we identified $CD90^+$ cells that were morphologically similar to VECs or fibroblasts within the tumor nodule in 37 of the 102 surgically resected HCC tissues (≥5% positive staining in a given area). IR to anti-CD90 Abs was also detected in hepatic mesenchymal tumors (Supporting Fig. 1C, panels a-c), indicating that CD90 is also a marker of liver stromal tumors.

Double-color IHC and immunofluorescence (IF) analysis confirmed the distinct expression of EpCAM and CD90 in HCC (Fig. 2B), consistent with the FACS data (Fig. 1A). Quantitative real-time polymerase chain reaction (qPCR) analysis of sorted $EpCAM^+$, $CD90^+$, and $EpCAM^-$ $CD90^-$ cells after $CD45^+$ cell depletion indicated that the hepatic stem/progenitor markers, *AFP* and *KRT19*, were up-regulated in $EpCAM^+$ cells (red bar), whereas the mesenchymal markers, *KIT* and *FLT1*, were up-regulated in $CD90^+$ cells (orange bar), compared with $EpCAM^-$ $CD90^-$ cells (blue bar) (Fig. 2C). The hepatocyte marker, *CYP3A4*, was down-regulated in $EpCAM^+$ cells and not detected in $CD90^+$ cells, compared with $EpCAM^-$ $CD90^-$ cells. *POU5F1* and *BMI1* were equally up-regulated in both $EpCAM^+$ and $CD90^+$ cells, compared with $EpCAM^-$ $CD90^-$ cells.

EpCAM and CD90 were independently and distinctively expressed in different cellular lineages, so we evaluated the staining of EpCAM and CD90 separately and analyzed the clinicopathological characteristics of surgically resected HCC cases. HCCs were regarded marker positive if ≥5% positive staining was detected in a given area. The existence of $EpCAM^+$

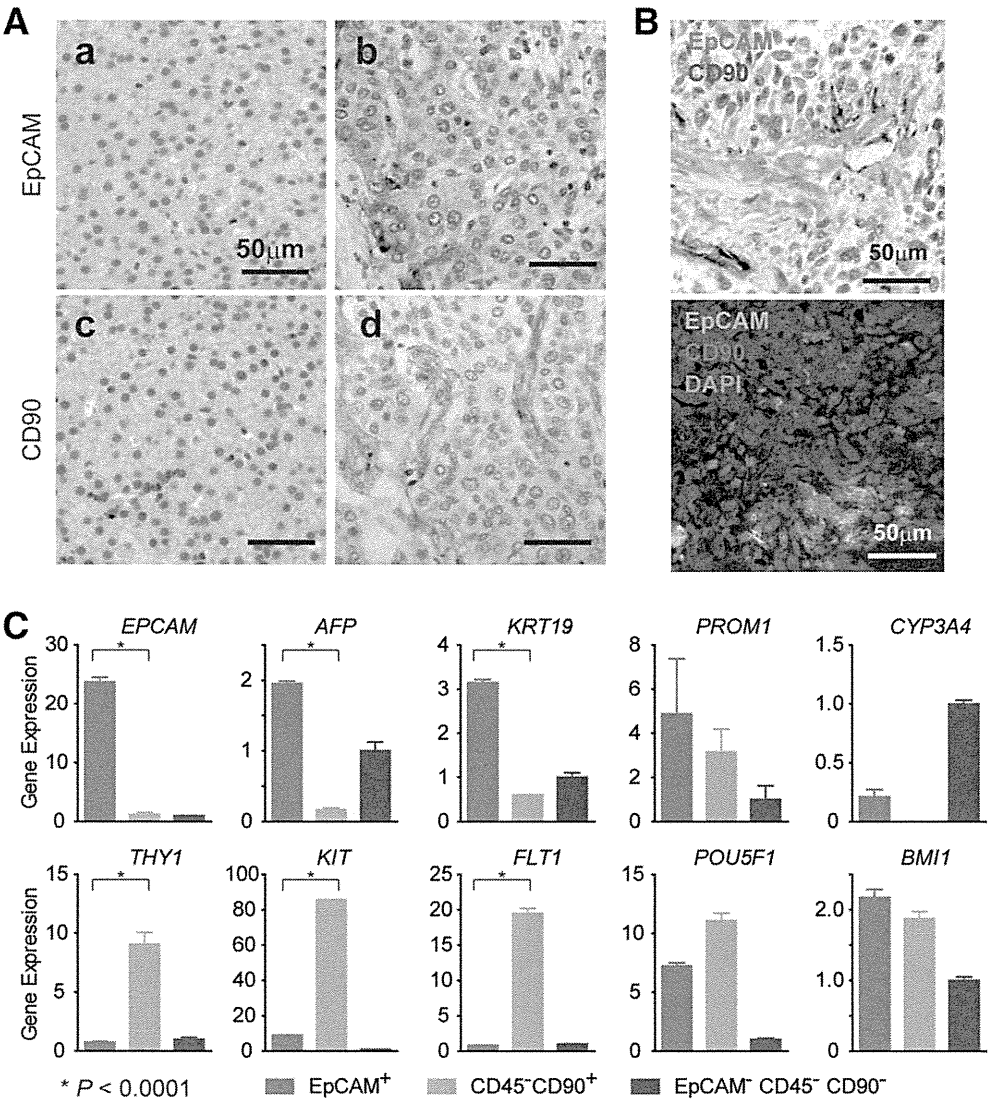

Fig. 2. Distinct EpCAM$^+$ and CD90$^+$ cell populations in HCC. (A) Representative images of EpCAM and CD90 staining in dysplastic nodule (panels a,c) and HCC (panels b,d) by IHC analysis (scale bar, 50 μm). EpCAM (panels a,b) and CD90 (panels c,d) immunostaining is depicted. (B) Upper panel: representative images of EpCAM (red) and CD90 (brown) double staining in HCC by IHC (scale bar, 50 μm). Lower panel: representative images of EpCAM (green) and CD90 (red) staining with 4'6-diamidino-phenylindole (DAPI) (blue) in HCC by IF (scale bar, 50 μm). (C) qPCR analysis of sorted EpCAM$^+$ (red bar), CD90$^+$ (orange bar), or EpCAM$^-$ CD90$^-$ (blue bar) derived from a representative primary HCC. Experiments were performed in triplicate, and data are shown as mean ± standard error of the mean.

cells (≥5%) was characterized by poorly differentiated morphology and high serum AFP values with a tendency for portal vein invasion, whereas the existence of CD90$^+$ cells (≥5%) was associated with poorly differentiated morphology and a tendency for large tumor size (Supporting Tables 2 and 3). Notably, the existence of CD90$^+$ cells was associated with a high incidence of distant organ metastasis, including lung, bone, and adrenal gland, within 2 years after surgery, whereas EpCAM$^+$ cell abundance appeared unrelated to distant organ metastasis.

We evaluated the characteristics of EpCAM$^+$ or CD90$^+$ cells in seven representative HCC cell lines. Morphologically, all EpCAM$^+$ cell lines (HuH1, HuH7, and Hep3B) showed a polygonal, epithelial cell shape, whereas three of four CD90$^+$ cell lines (HLE, HLF, and SK-Hep-1) showed a spindle cell shape (Fig. 3A). EpCAM$^+$ cells were detected in 11.5%, 57.7%, and 99.6% of sorted HuH1, HuH7, and Hep3B cells, respectively. A small CD90$^+$ cell population (0.66%) was observed in PLC/PRL/5, whereas 91.3%, 10.8%, and 59.0% of CD90$^+$ cells were detected in HLE, HLF, and SK-Hep-1, respectively. Compared with primary HCCs, only EpCAM$^+$ or CD90$^+$ cells were detected in liver cancer cell lines under normal culture conditions (Fig. 3B), suggesting that these cell lines contain a relatively pure cell population most likely obtained by clonal selection through the establishment process.

A class-comparison analysis with univariate t tests and a global permutation test (×10,000) of microarray data yielded two main gene clusters up-regulated in EpCAM$^+$ cell lines (HuH1, HuH7, and Hep3B) (cluster I, 524 genes) or in CD90$^+$ cell lines (HLE, HLF, and SK-Hep-1) (cluster II, 366 genes) (Fig. 3C). PLC/PRL/5 showed intermediate gene-expression patterns between EpCAM$^+$ and CD90$^+$ cell lines using this gene set. Pathway analysis indicated that the genes

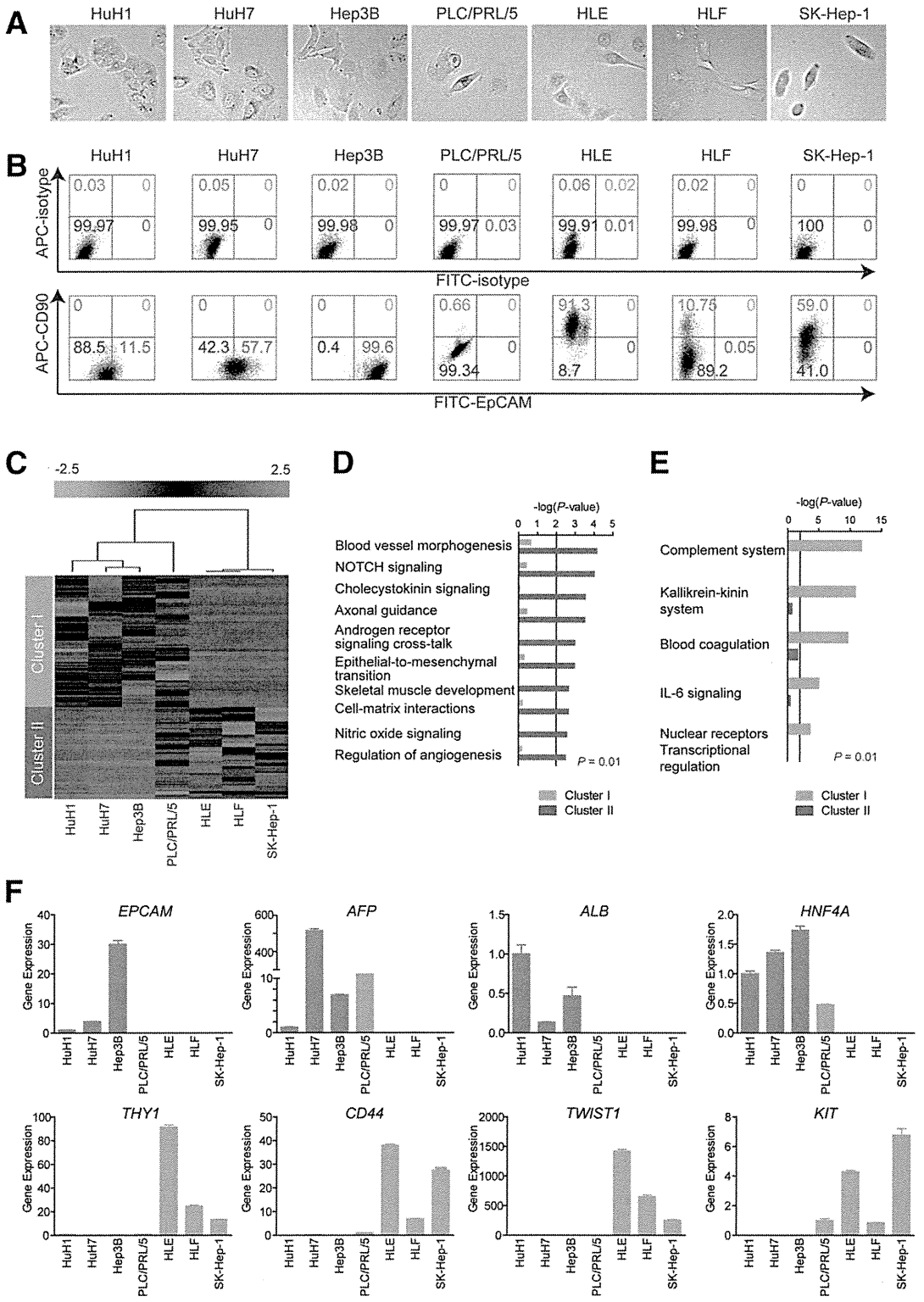

Fig. 3. Characteristics of HCC cell lines defined by EpCAM and CD90. (A) Representative photomicrographs of EpCAM^{+}CD90^{-} and EpCAM^{-} CD90^{+} HCC cell lines. (B) Representative FACS data of EpCAM^{+}CD90^{-} and EpCAM^{-} CD90^{+} HCC cell lines stained with fluorescein isothiocyanate (FITC)-EpCAM and APC-CD90 Abs. (C) Heat-map images of seven HCC cell lines based on 890 EpCAM/CD90-coregulated genes. Each cell in the matrix represents the expression level of a gene in an individual sample. Red and green cells depict high and low expression levels, respectively, as indicated by the scale bar. (D and E) Pathway analysis of EpCAM/CD90-coregulated genes. Canonical signaling pathways activated in cluster I (orange bar) or II (blue bar) with statistical significance ($P < 0.01$) are shown. (F) qPCR of representative differentially expressed genes identified by microarray analysis (C) in seven HCC cell lines.

enriched in cluster II were mainly associated with blood-vessel morpho- and angiogenesis (Fig. 3D). By contrast, the enriched genes in cluster I were significantly associated with known hepatocyte functions ($P < 0.01$) (Fig. 3E). In addition, we identified that the enriched genes in cluster II were significantly associated with neurogenesis, skeletal muscle development, and EMT.

We used qPCR to validate that known hepatic stem cell (HSC) and hepatocyte markers, such as *AFP*, *EPCAM*, *ALB*, and *HNF4A* genes, were up-regulated in $EpCAM^+$ cell lines, but not detected in $CD90^+$ cell lines (Fig. 3F). By contrast, genes associated with mesenchymal lineages and EMT, such as *KIT*, *TWIST1*, *CD44*, and *THY1*, were strongly up-regulated in $CD90^+$ cell lines.

Unique Tumorigenicity and Metastasis Capacity of Distinct CSCs Defined by EpCAM and CD90. We investigated the tumorigenic capacity of $EpCAM^+$ or $CD90^+$ cells by subcutaneously (SC) injecting 1×10^5 sorted cells of four HCC cell lines (HuH1, HuH7, HLE, and HLF) into nonobese diabetic, severe combined immunodeficient (NOD/SCID) mice. We excluded Hep3B cells for the evaluation of tumorigenicity because almost 100% of cells were EpCAM positive. We further excluded SK-Hep-1 cells from the analysis because they potentially originated from endothelial cells.[12] The highly tumorigenic capacities of $EpCAM^+$ and $CD90^+$ cells were reproduced in HuH1, HuH7, and HLF cell lines, compared with marker-negative cells (Fig. 4A). However, HLE cells did not produce SC tumors, even 12 months after transplantation, in NOD/SCID mice. $EpCAM^+$ cells from HuH1 and HuH7 formed larger tumors more rapidly than $CD90^+$ cells from HLF (Fig. 4B). IHC analyses indicated that $EpCAM^+$ cells did not produce $CD90^+$ cells and *vice versa* in these cell lines *in vivo* (Fig. 4C). $CD90^+$ cells showed a high metastatic capacity, whereas $EpCAM^+$ cells showed no metastasis to the lung when SC tumor volume reached approximately 2,000 (HuH1 and HuH7) or 700 mm^3 (HLF) (Fig. 4D). The high metastatic capacity of PLC/PRL/5 cells, which contain a small population of $CD90^+$ cells, was also confirmed after SC injection into NOD/SCID mice (data not shown). $CD90^+$ cells could divide to generate both $CD90^+$ and $CD90^-$ cells, and $CD90^+$ cells showed a high capacity to invade and form spheroids with overexpression of *TWIST1* and *TWIST2*, which are known to activate EMT programs in HLF cells (Supporting Fig. 2A-D).

We next evaluated the tumorigenic/metastatic capacity of $CD45^-$ tumor cells using 12 fresh primary HCC specimens (P1-P12) that had been surgically resected (Table 2). We further evaluated the tumorigenicity of EpCAM/CD90 sorted cells obtained from xenografts derived from primary HCCs (Supporting Fig. 3A). Of these, we confirmed the tumorigenicity of cancer cells obtained from six primary HCCs after SC injection into NOD/SCID mice within 3 months after transplantation (Fig. 5A; Table 2; Supporting Fig. 3B). $EpCAM^+$ cells derived from four HCCs (P4, P7, P13, and P14) showed highly tumorigenic capacities, compared with $EpCAM^-$ cells. $CD90^+$ cells derived from two HCCs showed equal (P12) or more-tumorigenic capacities (P15), compared with $CD90^-$ cells. Tumorigenicity of $EpCAM^+$ cells was observed in three hepatitis C virus (HCV)-related HCCs and an hepatitis B virus (HBV)-related HCC, whereas tumorigenicity of $CD90^+$ cells was observed in two HBV-related HCCs (Tables 1 and 2).

Using unsorted cells, we compared the frequency of $EpCAM^+$ and $CD90^+$ cells in primary and xenograft tumors and found that $EpCAM^+$ cells remained, but $CD90^+$ cells disappeared, in secondary tumors derived from P4 or P7, whereas $EpCAM^+$ cells disappeared, but $CD90^+$ cells remained, in secondary tumors derived from P12 (Fig. 5B). Morphologically, tumorigenic $EpCAM^+$ cells showed an epithelial cell shape, whereas $CD90^+$ cells showed a mesenchymal VEC shape (Fig. 5C and Supporting Fig. 3C). FACS analysis indicated that P12 HCC cells showed abundant expression of vascular endothelial growth factor receptor (VEGFR) 1 and a vascular endothelial marker endoglin (CD105) (Fig. 5D). By contrast, P4 and P7 HCC cells did not express these vascular endothelial markers (data not shown). Lung metastasis was detected in NOD/SCID mice transplanted with P12 HCC cells, but not in mice transplanted with P4 and P7 HCC cells (Fig. 5E,F).

Taken together, these results suggest that the tumorigenic and metastatic capability of primary HCC may depend on the presence of distinct $EpCAM^+$ or $CD90^+$ CSCs. $EpCAM^+$ cells were associated with a high tumorigenic capacity with hepatic epithelial stem cell features, whereas $CD90^+$ cells were related to the metastatic propensity with VEC features.

Suppression of Lung Metastasis Mediated by $CD90^+$ CSCs by Imatinib Mesylate. We previously demonstrated that Wnt/β-catenin signaling inhibitors could successfully attenuate the tumorigenic capacity of $EpCAM^+$ CSCs in HCC.[8,10] To explore the potential molecular targets activated in $CD90^+$ CSCs, we investigated the expression of the known VEC markers, CD105, VEGFR1 (encoded by *FLT1*), and

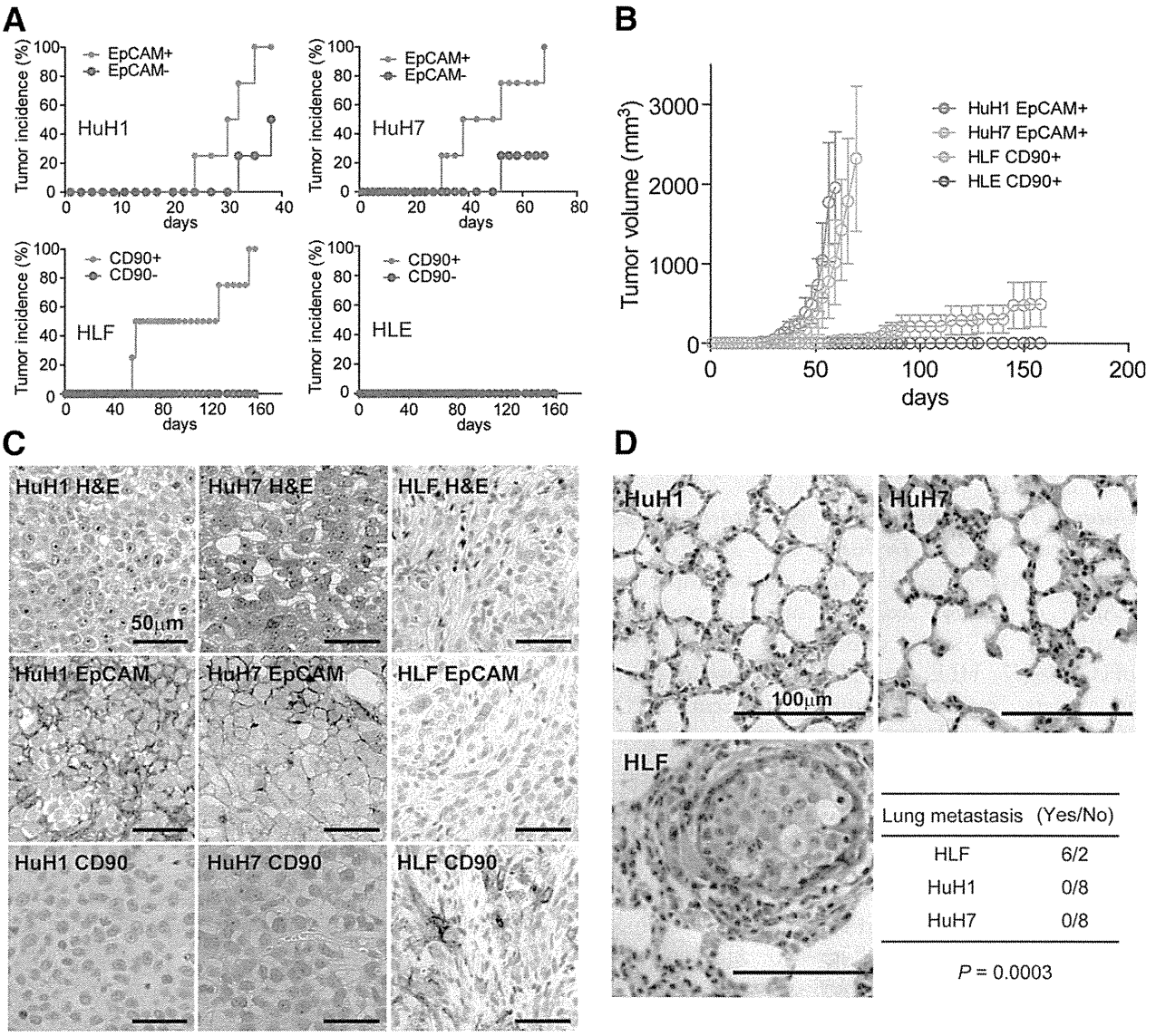

Fig. 4. Distinct tumorigenic/metastatic capacities of HCC cell lines defined by EpCAM and CD90. (A) Tumorigenicity of 1×10^5 cells sorted by anti-EpCAM (HuH1 and HuH7) or anti-CD90 (HLE and HLF) Abs. Data are generated from 8 mice/cell line. (B) Tumorigenic ability of $EpCAM^+$ and $CD90^+$ sorted cells in NOD/SCID mice. Aggressive tumor growth in the SC lesion was observed in $EpCAM^+$ HuH1 or HuH7 cells, compared with $CD90^+$ HLE or HLF cells. $EpCAM^+$ (1×10^5) or $CD90^+$ cells were injected. Tumor-volume curves are depicted as mean ± standard deviation of 4 mice/group. (C) Histological analysis of $EpCAM^+$ or $CD90^+$ cell-derived xenografts. Hematoxylin and eosin (H&E) staining of a SC tumor (upper panels) and IHC of the tumor with anti-EpCAM (middle panels) or anti-CD90 Abs (bottom panels) are shown (scale bar, 50 μm). (D) Metastasis was evaluated macroscopically and microscopically in the left and right lobes of the lung separately in each mouse (n = 4) (scale bar, 100 μm).

c-Kit (encoded by *KIT*), in cell lines and showed that they were abundantly expressed in $CD90^+$ cell lines, but not $EpCAM^+$ cell lines (Fig. 6A). No expression of VEGFR2 was detected in this set of cell lines, suggesting that molecular reagents specifically targeting VEGFR2 may have no effects on $CD90^+$ CSCs. CD44, a stem cell marker that functionally regulates redox status and is a potential target of $CD90^+$ CSCs, was also abundantly expressed in $CD90^+$ cell lines (Supporting Fig. 4A), consistent with previous data.[5,13] No significant difference was detected in the expression of the hematopoietic marker, CD34, or ABCG2 between $EpCAM^+$ and $CD90^+$ cell lines (Supporting Fig. 4A).

Among these molecular targets, we focused on the characterization of c-Kit because the c-Kit tyrosine kinase inhibitor, imatinib mesylate, is readily available, is widely used for the treatment of gastrointestinal stromal tumor with activation of c-Kit, and may have potential antitumor activity against a subset of HCC.[14] We explored the effect of imatinib mesylate on HCC cell lines and found that treatment with 10

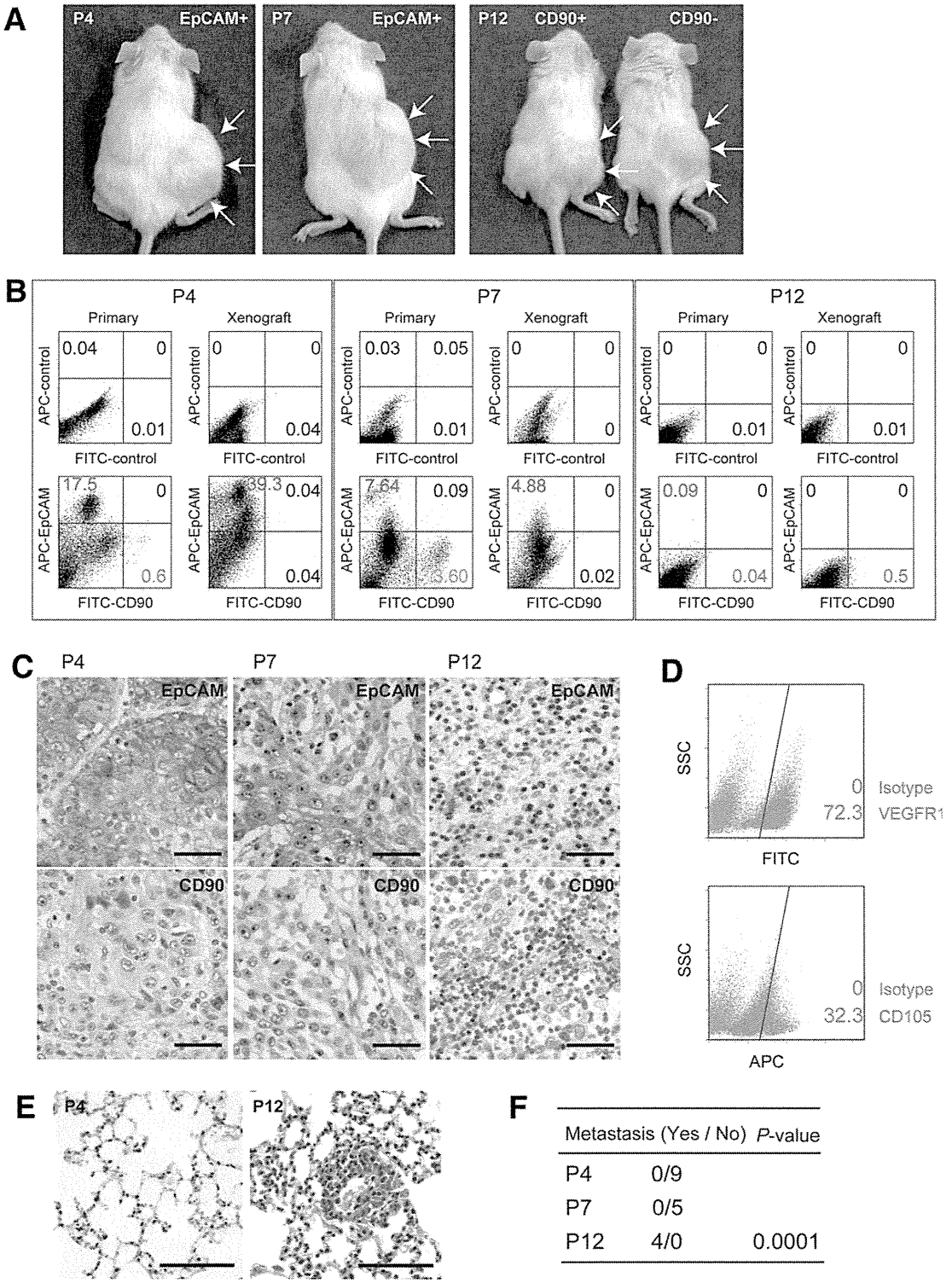

Fig. 5. Tumorigenic/metastatic capacities of EpCAM$^+$ and CD90$^+$ cells in primary HCC. (A) Representative NOD/SCID mice with SC tumors (white arrows) from EpCAM$^+$ P4 or P7 cells (left and middle panels) and CD90$^+$ or CD90$^-$ P12 cells (right panel). (B) FACS analysis of CD90 and EpCAM staining in primary HCCs and the corresponding secondary tumors developed in NOD/SCID mice. Unsorted cells (1×10^6 cells in P4 and P7 or 1×10^5 cells in P12) were SC injected to evaluate the frequency of each marker-positive cell in primary and secondary tumors. (C) IHC analysis of EpCAM and CD90 in primary HCCs P4, P7, and P12 (scale bar, 50 μm). (D) FACS analysis of VEGFR1 (Alexa488) and CD105 (APC) in primary HCC P12. (E) Hematoxylin and eosin staining of lung tissues in P4 and P12 (scale bar, 200 μm). (F) Frequency of lung metastasis in NOD/SCID mice SC transplanted using unsorted primary HCC cells.

μM reduced cell proliferation and spheroid formation in CD90$^+$ cell lines, but had no effect on EpCAM$^+$ cell lines (Supporting Fig. S4B,C).

We further explored the effect of imatinib mesylate *in vivo*. Because EpCAM$^+$ and CD90$^+$ cells reside in the primary HCC, but not in established cell lines, we SC injected HuH7 and HLF cell lines to generate tumors organized by EpCAM$^+$ and CD90$^+$ CSCs. Interestingly, when HLF cells were coinjected with HuH7 cells, EpCAM$^+$ cells could metastasize to the lung, whereas

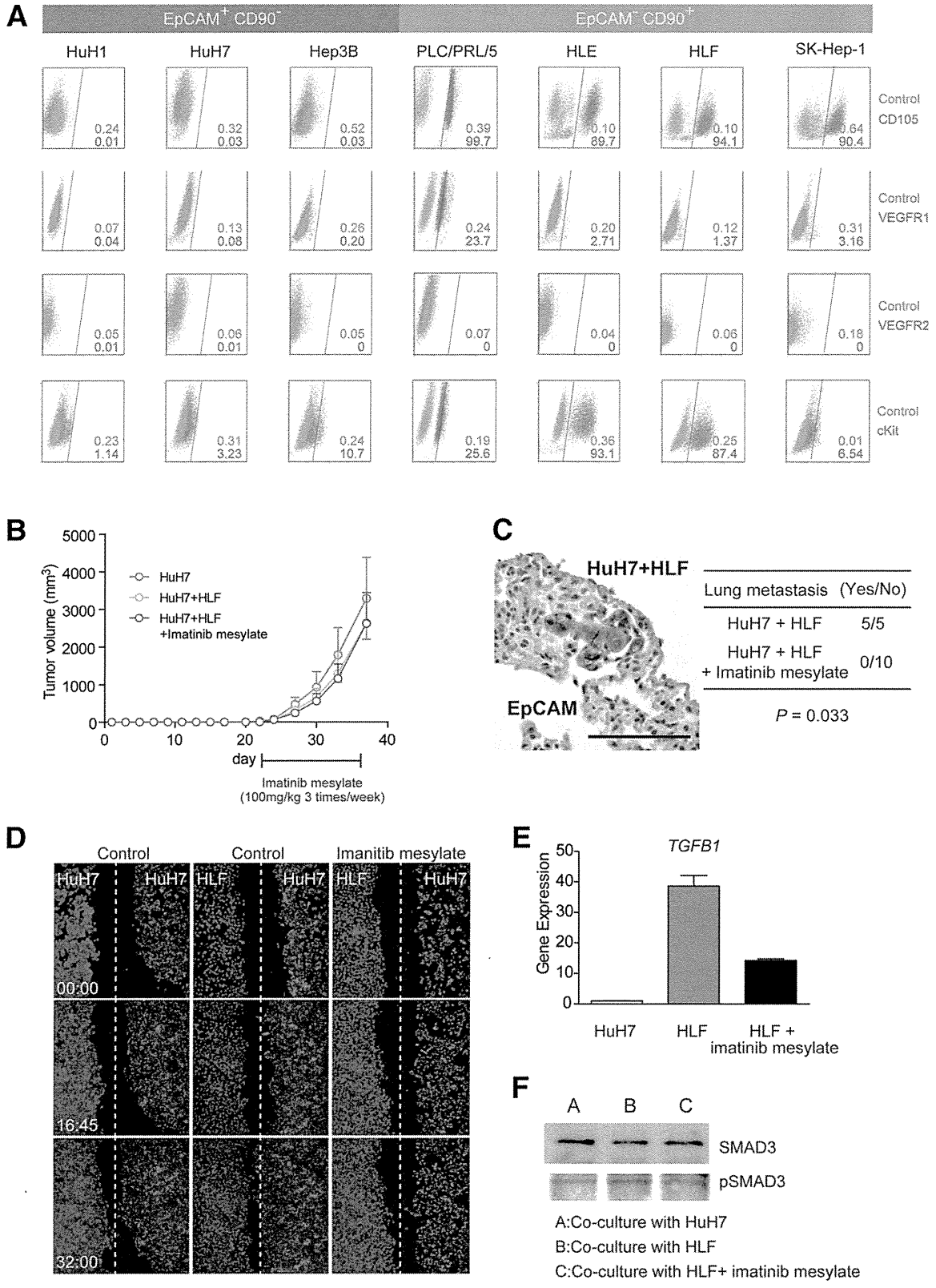

Fig. 6.

SC primary tumors showed no difference in size (Fig. 6B,C). Furthermore, although imatinib mesylate treatment had little effect on the size of primary SC tumors, it significantly suppressed lung metastasis in primary tumors (Fig. 6C). These data suggest that $CD90^+$ cells are not only metastatic to the distant organ, but also help the metastasis of $CD90^-$ cells, including $EpCAM^+$ cells, which originally have no distant metastatic capacity. Our data further suggest that imatinib mesylate can inhibit distant organ metastasis by suppressing $CD90^+$ metastatic CSCs, albeit with little effect on $EpCAM^+$ tumorigenic epithelial stem-like CSCs.

To explore the potential mechanism of how $CD90^+$ cells dictate the metastasis of $EpCAM^+$ cells, we utilized coculture systems and time-lapse image analysis. Wound-healing analysis clearly indicated that motility of HuH7 cells was enhanced when HLF cells were cocultured, and this effect was abolished by imatinib mesylate treatment (Fig. 6D; see Supporting Videos 1-3). HLF cells abundantly expressed *TGFB1*, compared with HuH7 cells, and its expression was dramatically suppressed by imatinib mesylate treatment (Fig. 6E). Mothers against decapentaplegic homolog 3 (Smad3) phosphorylation was augmented in HuH7 cells when cocultured with HLF cells, and this effect was attenuated when cocultured with HLF cells pretreated with imatinib mesylate.

Taken together, our data suggest that liver CSCs are not a single entity. Liver CSCs defined by different markers show unique features of tumorigenicity/metastasis with phenotypes closely associated with committed liver lineages. These distinct CSCs may collaborate to enhance tumorigenicity and metastasis of HCCs.

Discussion

The current investigation demonstrates that CSC marker expression status may be a key determinant of cancer phenotypes, in terms of metastatic propensity and chemosensitivity, to certain molecularly targeted therapies. EpCAM appears to be an epithelial tumorigenic CSC marker, whereas CD90 seems to be a mesenchymal metastatic CSC marker associated with expression of c-Kit and chemosensitivity to imatinib mesylate. Imatinib mesylate may be effective in inhibiting metastasis, but has little effect on primary $EpCAM^+$ HCC cell growth.

We investigated the frequency of three CSC markers (EpCAM, CD90, and CD133) in 15 primary HCCs with a confirmed cell viability of $\geq$70% and found that three HCCs contained $CD133^+$ cells, seven HCCs contained $EpCAM^+$ cells, and all HCCs contained $CD90^+$ cells. Among them, we confirmed the perpetuation of $CD133^+$ cells derived from three HCCs (P7, P12, and P14; data not shown), $EpCAM^+$ cells derived from four HCCs (P4, P7, P13, and P14), and $CD90^+$ cells derived from two HCCs (P12 and P15). Recent studies showed that at least 8 of 21 HCCs (38%)[4] and 13 of 13 HCCs (100%)[5] contained tumorigenic $CD133^+$ or $CD90^+$ CSCs, respectively. Recent IHC and tissue microarray studies also demonstrated that $CD133^+$ and $CD90^+$ cells were detected in 24.8% ($\geq$1% of tumor cells) and 32.2% ($\geq$5% of tumor cells) of HCC cases examined, respectively.[15,16]

One possible explanation of the comparatively low frequency of $CD133^+$ liver CSCs identified in our study is that we used the monoclonal Ab CD133/2, whereas Ma et al. used CD133/1. Another possible explanation is the difference of etiology related to hepatocarcinogenesis. We examined tumorigenicity using 15 HCCs (five HBV related, four HCV related, three non-B, non-C hepatitis [NBNC] related, and three alcohol related) and identified that tumorigenic CSCs were only obtained from HBV- or HCV-related cases. Previous liver CSC studies were performed using HBV-related HCCs,[4,5] and a recent study showed that

Fig. 6. Suppression of lung metastasis mediated by $CD90^+$ CSCs by imatinib mesylate. (A) FACS analysis of seven HCC cell lines stained by APC-CD105, Alexa 488/VEGFR1, APC/VEGFR2, and Alexa 488/c-Kit Abs or isotype control. (B) Tumorigenicity of 5×10^5 HuH7 cells and 2.5×10^5 HuH7 cells plus 2.5×10^5 HLF cells treated with imatinib mesylate or control phosphate-buffered saline (PBS) (200 μL/mouse) orally ingested three times per week (100 mg/kg) for 2 weeks. Data are generated from 5 mice per condition. (C) IHC analysis of EpCAM in lung metastasis detected in NOD/SCID mice SC injected with 2.5×10^5 HuH7 cells and 2.5×10^5 HLF cells. Metastasis was evaluated macro- and microscopically in the left and right lobes of the lung separately in each mouse ($n = 5$) (scale bar, 100 μm). (D) Cell motility of HuH7 cells cocultured with HuH7, HLF, or HLF cells with imatinib mesylate (10 μM) was monitored in a real-time manner by time-lapse image analysis. HuH7 and HLF cells were labeled with the lipophilic fluorescence tracer, DiI (indicated as red) or DiD (indicated as blue), and incubated in a μ-Slide eight-well chamber overnight. Silicone inserts were detached and the culture media replaced with Dulbecco's modified Eagle's medium containing 10% fetal bovine serum, including 0.1% dimethyl sulfoxide (DMSO) (control) or 10 μM of imatinib mesylate dissolved in DMSO (final concentration 0.1%). Immediately after the medium change, cells were cultured at 37°C in 5% CO_2 and time-lapse images were captured for 72 hours. (E) qPCR analysis of *TGFB1* in HuH7 (white bar), HLF (gray bar), and HLF cells pretreated with imatinib mesylate for 24 hours. (F) Smad3 and its phosphorylation evaluated by western blotting. HuH7 cells and HLF cells were harvested in cell culture inserts and treated with DMSO (0.1%) or imatinib mesylate (10 μM) for 24 hours. Cell culture inserts were washed with PBS, cocultured with HuH7 cells for 8 hours, and then removed. HuH7 cells were lysed using radioimmunoprecipitation assay buffer for western blotting. (A) HuH7 cells cocultured with HuH7 cells. (B) HuH7 cells cocultured with HLF cells. (C) HuH7 cells cocultured with HLF cells pretreated with imatinib mesylate.

HBV X may play a role in generating $EpCAM^+$ CSCs.[17] The role of hepatitis virus infection on the generation of CSCs is still unclear and should be clarified in future studies.

We were unable to confirm the tumorigenicity of $CD90^+$ cells in 13 of 15 HCCs, but we observed abundant $CD90^+$ cells in more-advanced HCCs by IHC (data not shown). Tumorigenic $CD90^+$ cells may emerge at a later stage of hepatocarcinogenesis, and the majority of $CD90^+$ cells in early HCCs may be cancer-associated VECs without tumorigenic capacity. Furthermore, we identified tumorigenic $CD90^+$ cells only from HBV-related HCCs, and a recent study suggested that expression of CD90 was associated with HBV infection.[16] We could not detect the small population of $CD90^+$ HuH7 and Hep3B cells reported on by Yang et al. However, because we identified a small population of $CD90^+$ HuH7 cells after treatment with 5-FU (manuscript in preparation), it is conceivable that different cellular stress statuses may explain the observed differences between our findings and those of Yang et al.

The majority of CSC markers discovered thus far are almost identical to those found in healthy tissue stem cells or embryonic stem cells. However, with regard to the liver, the characteristics of healthy hepatic stem/progenitor cells isolated using different stem cell markers are currently under investigation. A recent article examined the characteristics of $EpCAM^+$ and $CD90^+$ oval cells isolated from 2-acetylaminofluorene/partial hepatectomy or D-galactosamine-treated rats.[18] Interestingly, $EpCAM^+$ and $CD90^+$ oval cells represent two distinct populations: The former expresses classical oval cell markers, such as AFP, OV-1, and cytokeratin-19 (CK-19), whereas the latter expresses desmin and alpha smooth muscle actin, but not AFP, OV-1, or CK-19, which indicates that $CD90^+$ populations are more likely to be mesenchymal cells. Another study has demonstrated that mesenchymal cells can interact with HSCs to regulate cell-fate decision.[19] We found that $EpCAM^+$ and $CD90^+$ cells isolated from liver cancer are distinct in terms of gene- and protein-expression patterns in both primary liver cancers and cell lines. Furthermore, these distinct CSCs can interact to regulate the tumorigenicity and metastasis of HCC. Molecular characteristics of $EpCAM^+/CD90^+$ CSCs may potentially reflect the cellular context of healthy stem or progenitor cells.

Although our study strongly indicates that abundant $CD90^+$ cells in a tumor is a risk for distant metastasis in liver cancer, the cell identity and role of $CD90^+$ cells remains elusive. As our IHC, FACS, and xenotransplantation assays revealed, some $CD90^+$ cells in liver cancer may be cancer-associated VECs or fibroblasts that cannot perpetuate in the xenograft. Recent findings have suggested the importance of stromal cells in tumorigenesis and cancer metastasis,[20-22] so it is possible that these cells may help TECs invade and intravasate into blood vessels, thus playing crucial roles in metastasis.

Another possibility is that $CD90^+$ cells are cancer cells with features of fibroblasts (having undergone EMT) or VECs (having undergone vasculogenic mimicry; VM) that can invade, intravasate, and metastasize cells to distant organs. Recently, two groups reported that a subset of tumor VECs originate from glioblastoma CSCs.[23,24] We successfully confirmed the tumorigenicity and metastatic capacity of $CD90^+$ cells that were morphologically identical to VECs from primary HCCs that could perpetuate in the xenograft. However, a recent study demonstrated that $CD90^+$ HCC cells express glypican-3, a marker detected in hepatic epithelial cells.[25] Further studies are warranted to clarify the nature and role of $CD90^+$ HCC cells.

In our study, $CD90^+$ cells expressed the endothelial marker, c-Kit, CD105, and VEGFR1, and a mesenchymal VEC morphology and high metastatic capacity were confirmed in both primary liver cancer and cell lines. We further confirmed that $CD90^+$ liver cancer cells showed chemosensitivity to imatinib mesylate, suggesting that cancer cells committed to mesenchymal endothelial lineages could be eradicated by the compound. Although imatinib mesylate treatment had little effect on the size of primary tumors originated from both $EpCAM^+$ and $CD90^+$ CSCs, it significantly suppressed lung metastasis *in vivo*. These data are consistent with a recent phase II study demonstrating the tolerable toxicity, but limited efficacy, of imatinib mesylate alone for unresectable HCC patients. Eligibility of imatinib mesylate for advanced HCC patients may be restricted to the HCC subtypes organized by $CD90^+$ CSCs with a highly metastatic capacity and VEC features. Therefore, a combination of compounds targeting $EpCAM^+$ tumorigenic CSCs as well as $CD90^+$ metastatic CSCs may be required for the eradication of HCC and should be tested in the future.

Acknowledgments: The authors thank Ms. Nami Nishiyama and Ms. Mikiko Nakamura for their excellent technical assistance.

References

1. Tsai WL, Chung RT. Viral hepatocarcinogenesis. Oncogene 2010;29: 2309-2324.

2. Chiba T, Kita K, Zheng YW, Yokosuka O, Saisho H, Iwama A, et al. Side population purified from hepatocellular carcinoma cells harbors cancer stem cell-like properties. HEPATOLOGY 2006;44:240-251.
3. Haraguchi N, Ishii H, Mimori K, Tanaka F, Ohkuma M, Kim HM, et al. CD13 is a therapeutic target in human liver cancer stem cells. J Clin Invest 2010;120:3326-3339.
4. Ma S, Tang KH, Chan YP, Lee TK, Kwan PS, Castilho A, et al. miR-130b promotes CD133(+) liver tumor-initiating cell growth and self-renewal via tumor protein 53-induced nuclear protein 1. Cell Stem Cell 2010;7:694-707.
5. Yang ZF, Ho DW, Ng MN, Lau CK, Yu WC, Ngai P, et al. Significance of CD90+ cancer stem cells in human liver cancer. Cancer Cell 2008;13:153-166.
6. Zen Y, Fujii T, Yoshikawa S, Takamura H, Tani T, Ohta T, Nakanuma Y. Histological and culture studies with respect to ABCG2 expression support the existence of a cancer cell hierarchy in human hepatocellular carcinoma. Am J Pathol 2007;170:1750-1762.
7. Lee TK, Castilho A, Cheung VC, Tang KH, Ma S, Ng IO. CD24(+) liver tumor-initiating cells drive self-renewal and tumor initiation through STAT3-mediated NANOG regulation. Cell Stem Cell 2011;9: 50-63.
8. Yamashita T, Budhu A, Forgues M, Wang XW. Activation of hepatic stem cell marker EpCAM by Wnt-beta-catenin signaling in hepatocellular carcinoma. Cancer Res 2007;67:10831-10839.
9. Yamashita T, Forgues M, Wang W, Kim JW, Ye Q, Jia H, et al. EpCAM and alpha-fetoprotein expression defines novel prognostic subtypes of hepatocellular carcinoma. Cancer Res 2008;68:1451-1461.
10. Yamashita T, Ji J, Budhu A, Forgues M, Yang W, Wang HY, et al. EpCAM-positive hepatocellular carcinoma cells are tumor-initiating cells with stem/progenitor cell features. Gastroenterology 2009;136: 1012-1024.
11. Ma S, Chan KW, Hu L, Lee TK, Wo JY, Ng IO, et al. Identification and characterization of tumorigenic liver cancer stem/progenitor cells. Gastroenterology 2007;132:2542-2556.
12. Heffelfinger SC, Hawkins HH, Barrish J, Taylor L, Darlington GJ. SK HEP-1: a human cell line of endothelial origin. In Vitro Cell Dev Biol 1992;28A:136-142.
13. Ishimoto T, Nagano O, Yae T, Tamada M, Motohara T, Oshima H, et al. CD44 variant regulates redox status in cancer cells by stabilizing the xCT subunit of system xc(-) and thereby promotes tumor growth. Cancer Cell 2011;19:387-400.
14. Ramadori G, Fuzesi L, Grabbe E, Pieler T, Armbrust T. Successful treatment of hepatocellular carcinoma with the tyrosine kinase inhibitor imatinib in a patient with liver cirrhosis. Anticancer Drugs 2004;15: 405-409.
15. Kim H, Choi GH, Na DC, Ahn EY, Kim GI, Lee JE, et al. Human hepatocellular carcinomas with "Stemness"-related marker expression: keratin 19 expression and a poor prognosis. HEPATOLOGY 2011;54: 1707-1717.
16. Lu JW, Chang JG, Yeh KT, Chen RM, Tsai JJ, Hu RM. Overexpression of Thy1/CD90 in human hepatocellular carcinoma is associated with HBV infection and poor prognosis. Acta Histochem 2011;113: 833-838.
17. Arzumanyan A, Friedman T, Ng IO, Clayton MM, Lian Z, Feitelson MA. Does the hepatitis B antigen HBx promote the appearance of liver cancer stem cells? Cancer Res 2011;71:3701-3708.
18. Yovchev MI, Grozdanov PN, Zhou H, Racherla H, Guha C, Dabeva MD. Identification of adult hepatic progenitor cells capable of repopulating injured rat liver. HEPATOLOGY 2008;47:636-647.
19. Wang Y, Yao HL, Cui CB, Wauthier E, Barbier C, Costello MJ, et al. Paracrine signals from mesenchymal cell populations govern the expansion and differentiation of human hepatic stem cells to adult liver fates. HEPATOLOGY 2010;52:1443-1454.
20. Dome B, Timar J, Ladanyi A, Paku S, Renyi-Vamos F, Klepetko W, et al. Circulating endothelial cells, bone marrow-derived endothelial progenitor cells and proangiogenic hematopoietic cells in cancer: from biology to therapy. Crit Rev Oncol Hematol 2009;69:108-124.
21. Karnoub AE, Dash AB, Vo AP, Sullivan A, Brooks MW, Bell GW, et al. Mesenchymal stem cells within tumour stroma promote breast cancer metastasis. Nature 2007;449:557-563.
22. Mishra PJ, Humeniuk R, Medina DJ, Alexe G, Mesirov JP, Ganesan S, et al. Carcinoma-associated fibroblast-like differentiation of human mesenchymal stem cells. Cancer Res 2008;68:4331-4339.
23. Ricci-Vitiani L, Pallini R, Biffoni M, Todaro M, Invernici G, Cenci T, et al. Tumour vascularization via endothelial differentiation of glioblastoma stem-like cells. Nature 2010;468:824-828.
24. Wang R, Chadalavada K, Wilshire J, Kowalik U, Hovinga KE, Geber A, et al. Glioblastoma stem-like cells give rise to tumour endothelium. Nature 2010;468:829-833.
25. Ho DW, Yang ZF, Yi K, Lam CT, Ng MN, Yu WC, et al. Gene expression profiling of liver cancer stem cells by RNA-sequencing. PLoS One 2012;7:e37159.

HEPATOLOGY
Official Journal of the American Association for the Study of Liver Diseases

Enhancement of Tumor-Associated Antigen-Specific T Cell Responses by Radiofrequency Ablation of Hepatocellular Carcinoma

Eishiro Mizukoshi, Tatsuya Yamashita, Kuniaki Arai, Hajime Sunagozaka, Teruyuki Ueda, Fumitaka Arihara, Takashi Kagaya, Taro Yamashita, Kazumi Fushimi, and Shuichi Kaneko

Radiofrequency ablation (RFA) is one of the treatments for hepatocellular carcinoma (HCC) and is known to enhance host immune response. However, the epitopes to which enhanced immune responses occur, the impact on patient prognosis, and the functions and phenotype of T cells induced are still unclear. To address these issues, we analyzed immune responses before and after RFA in 69 HCC patients using 11 tumor-associated antigen (TAA)-derived peptides that we identified to be appropriate to analyze HCC-specific immune responses. The immune responses were analyzed using enzyme-linked immunospot (ELISPOT) assay and tetramer assays using peripheral blood mononuclear cells. An increase in the number of TAA-specific T cells detected by interferon-γ ELISPOT assays occurred in 62.3% of patients after RFA. The antigens and their epitope to which enhanced T cell responses occur were diverse, and some of them were newly induced. The number of TAA-specific T cells after RFA was associated with the prevention of HCC recurrence, and it was clarified to be predictive of HCC recurrence after RFA by univariate and multivariate analyses. The number of TAA-specific T cells after RFA was inversely correlated with the frequency of $CD14^{+}HLA\text{-}DR^{-/low}$ myeloid-derived suppressor cells (MDSCs). The modification of T cell phenotype was observed after RFA. The number of TAA-specific T cells at 24 weeks after RFA was decreased. *Conclusion*: Although RFA can enhance various TAA-specific T cell responses and the T cells induced contribute to the HCC recurrence-free survival of patients, besides immunosuppression by MDSCs, the memory phenotype and lifetime of TAA-specific T cells are not sufficient to prevent HCC recurrence completely. Additional treatments by vaccine or immunomodulatory drugs might be useful to improve the immunological effect of RFA. (HEPATOLOGY 2013; 57:1448-1457)

Hepatocellular carcinoma (HCC) is the sixth most frequent type of cancer worldwide, and it is becoming an important public health concern due to its increased incidence in Western and Asian countries.[1,2] Although there are many types of treatments for HCC, the posttreatment recurrence rate is very high.[3] To inhibit HCC recurrence and improve prognosis, an immunotherapeutic approach is considered an attractive strategy.

Radiofrequency ablation (RFA) is one of the treatments for HCC and is now widely used for curative strategies.[4] In recent studies, it has been reported that

Abbreviations: AFP, alpha-fetoprotein; CMV, cytomegalovirus; CT, computed tomography; ELISPOT, enzyme-linked immunospot; HCV, hepatitis C virus; HIV, human immunodeficiency virus; HLA, human leukocyte antigen; IFN-γ, interferon-γ; MDSC, myeloid-derived suppressor cell; MRI, magnetic resonance imaging; PBMC, peripheral blood mononuclear cell; RFA, radiofrequency ablation; TAA, tumor-associated antigen.

From the Department of Gastroenterology, Graduate School of Medicine, Kanazawa University, Kanazawa, Japan.

Received January 4, 2012; accepted October 23, 2012.

Supported in part by grants from the Ministry of Education, Culture, Sports, Science and Technology of Japan.

Address reprint requests to: Shuichi Kaneko, M.D., Department of Gastroenterology, Graduate School of Medicine, Kanazawa University, Kanazawa, Ishikawa 920-8641, Japan. E-mail: skaneko@m-kanazawa.jp; fax: (81)-76-234-4250.

View this article online at wileyonlinelibrary.com.

DOI 10.1002/hep.26153

Potential conflict of interest: Nothing to report.

Additional Supporting Information may be found in the online version of this article.